Coral Reefs and Sea-Level Change: Quaternary Records and Modelling

Edited by
Gilbert F. Camoin
and Nadine Hallmann

Series Editor
Elias Samankassou

Special Publication 49
of the International
Association of
Sedimentologists

IAS
INTERNATIONAL ASSOCIATION OF SEDIMENTOLOGISTS

IAS (2022) Coral Reefs and Sea-Level Change: Quaternary Records and Modelling, 215–273

Coral reef development and sea-level changes over the past 50,000 years: new evidence from the north-west shelf of Australia

JODY M. WEBSTER[*], BELINDA DECHNIK[*], KELSEY SANBORN[*], YUSUKE YOKOYAMA[†], JUAN CARLOS BRAGA[‡], WILLEM RENEMA[§], MARC HUMBLET[¶], ROBIN J. BEAMAN[|], LUKE D. NOTHDURFT[#], GREGORY E. WEBB[a], JIAN-XIN ZHAO[a], RICHARD J. MURPHY[*], STEPHEN J. GALLAGHER[b], MICHAEL O'LEARY[c] and VICTORIEN PAUMARD[c]

[*]*Geocoastal Research Group, University of Sydney, Sydney, Australia.*
[†]*Atmosphere and Ocean Research Institute and Department of Earth and Planetary Sciences, The University of Tokyo, Kashiwanoha, Japan.*
[‡]*Departamento de Estratigrafía y Paleontología, Universidad de Granada, Granada, Spain.*
[§]*Naturalis Biodiversity Center, Leiden, The Netherlands & Department of Ecosystem & Landscape Dynamics, Institute for Biodiversity & Ecosystem Dynamics, University of Amsterdam, Amsterdam, The Netherlands.*
[¶]*Department of Earth and Planetary Sciences, Nagoya University, Nagoya, Japan.*
[|]*College of Science and Engineering, James Cook University, Cairns, Queensland, Australia.*
[#]*School of Earth and Atmospheric Sciences, Queensland University of Technology, Brisbane, Australia.*
[a]*School of Earth and Environmental Sciences, The University of Queensland, Brisbane, Australia.*
[b]*School of Geography, Earth and Atmospheric Sciences, The University of Melbourne, Melbourne, Australia.*
[c]*Centre for Energy Geoscience, School of Earth Sciences, The University of Western Australia, Perth, Australia.*

ABSTRACT

Understanding of global sea-level changes and coral reef development is poorly constrained during Marine Isotope Stage 3 (MIS 3; ~60 to 30 ka). Australia's North West Shelf (NWS), at depths of ~50 to 120 m below present sea-level (mbsl), represents an ideal natural laboratory to address these knowledge gaps. In this study, the authors investigate a unique suite of sea-bed rock drill (PROD) cores recovered as part of a geotechnical survey from the NWS ~150 km south-east of Ashmore Reef. Twenty cores, penetrating to 28 m below sea floor, were collected from the top of the now drowned platform complex in similar water depths (74.8 to 81.6 mbsl), forming two transects ~17 km apart. High-resolution 3D seismic and multibeam bathymetry data reveal three distinct, multigenerational platforms that are rimmed by smaller reef terraces and bisected by deeper channels, placing the core transects into a robust, regional geomorphic context that includes a succession of linear palaeo-shorelines and tidal-estuarine channel systems on the adjacent shelf between ~90 to 110 mbsl. The authors have completed detailed logging, high-spatial resolution hyperspectral scanning, petrologic, mineralogic and sedimentary facies analysis of these cores, including a precise palaeoenvironmental reconstruction based on coral, algal and larger benthic foraminifera assemblages; and extensive radiometric dating. The authors have observed a complex suite of

lithologies including *in situ* coralgal reef frameworks, well-lithified to friable grainstones, packstones and coralline algal floatstone facies separated by at least two major palaeosol horizons. Together with thirty ^{14}C-AMS and closed-system U/Th ages spanning 10.7 to >50 ka, the authors define a complex but consistent record of four distinct chrono-stratigraphic units (Units 1 to 4), representing a repeated succession of shallow reef to deep reef-slope depositional settings as the platforms experienced repeated sea-level oscillations (interstadial/stadial to glacial/deglacial) over the last 75,000 yr. Two distinct phases of shallow-water, high-energy reef development are defined. The age of the older, diagenetically distinct reef unit (Unit 3) is unknown but interpreted to have developed before the MIS 4 lowstand (~65 ka). However, firm chronological constraints on the MIS 3 development of the younger reef unit (Unit 2), place the position of relative sea-level (RSL) between ~63 to 75 $\pm$ 1.8 mbsl by 45.95 to 39.23 $\pm$ 0.2 ka, consistent with other predictions and observations for the region. Following its exposure and demise due to sea-level fall to the Last Glacial Maximum (LGM), the platform system was unable to re-establish fully as it was reflooded during the subsequent deglacial sea-level rise. Deeper reef slope (Unit 1) facies dominate the core tops between ~13.2 to 10.7 ka, representing a major hiatus in shallow-water reef development on the platforms. Deglacial sea-level rise was either too fast and/or other environmental conditions inadequate (i.e. massive riverine sediment flux due to the strengthening Australian summer monsoon and/or reworking of shelf sediments) to allow re-establishment of shallow-water coral reef development on the platforms apart from a few isolated and distal locations (i.e. Ashmore, Cartier, Adele and Scott Reefs).

INTRODUCTION

Considerable progress has been made in understanding the role of coral reef systems as valuable archives of Quaternary sea-level and environmental changes and also how reefs were impacted by these changes (Woodroffe & Webster, 2014; Camoin & Webster, 2015; Gischler, 2015; Braithwaite, 2016). However, major questions still remain about: (1) what processes control high-resolution temporal and spatial variations in reef architecture and composition, particularly in response to millennial scale sea-level and climate changes (Blanchon *et al.*, 2009; Webster *et al.*, 2018), (2) what causes reefs to 'turn-on' or 'turn-off' (i.e. drowning and/or exposure) and what are their climatic and ecologic thresholds (Kiessling *et al.*, 2012; Toth *et al.*, 2015); and (3) how reef communities reassemble following disturbances on interglacial/glacial *vs* inter-stadial/stadial, millennial scales (Tager *et al.*, 2010; Precht & Aronson, 2016). There is an urgent need for further research, not only to decipher processes driving past sea-level and climate change and its geographical variability but also to better understand how coral reefs might respond in the context of future global climate change (Camoin & Webster, 2015).

Marine Isotope Stage 3 (MIS 3; 60 to 29 ka) is characterised by considerable millennial scale global sea-level and climate variability (Siddall *et al.*, 2008; Grant *et al.*, 2012) and therefore represents a key time period to gauge coral reef responses. However, well-dated MIS 3 reef records are rare and mainly limited to rapidly uplifting convergent margins such as the raised reef terraces on the Huon Peninsula, Papua New Guinea (PNG; Yokoyama *et al.*, 2000;

Yokoyama *et al.*, 2001; Chappell, 2002; Cutler *et al.*, 2003), Kikai-jima, Ryukyus (Sasaki *et al.*, 2004), Espiritu Santo and offshore islands, Vanuatu (Fairbanks *et al.*, 2005; Taylor *et al.*, 2005) or the few submerged reefs that have been sampled via scientific drilling or ROV at Barbados (Peltier & Fairbanks, 2006), Ryukyus (Sasaki *et al.*, 2006), Huon Gulf, PNG (Webster *et al.*, 2009), Tahiti (IODP Exp. 310; Thomas *et al.*, 2009) and most recently the Great Barrier Reef (GBR) (IODP Exp. 325; Gischler *et al.*, 2013; Webster *et al.*, 2018; Yokoyama *et al.*, 2018). Unfortunately, these records are either potentially biased by abrupt co-seismic uplift/subsidence events, chronologically poorly constrained, lack sufficient stratigraphic and multi-proxy coralgal data to allow accurate palaeoenvironmental reconstruction, and/or come from only one or few drill/ROV sites and not the closely spaced transects necessary to faithfully reconstruct MIS 3 reef growth modes, architecture and communities (Camoin & Webster, 2015).

Significant advances have been made in reconstructing sea-level changes over the past 150 kyrs using continuous deep-sediment archives (i.e. Grant *et al.*, 2012) and discontinuous fossil coral reefs that can provide more accurate constraints on the vertical position of past sea-level (Woodroffe & Webster, 2014). This has contributed to the understanding of eustatic sea-level (ESL) variability, ice sheet dynamics and global isostatic adjustment (GIA) over the last 150 ka, particular during MIS 5e (Dutton *et al.*, 2015) and the LGM-deglaciation (IODP Exp. 310, 325; Barbados; Deschamps *et al.*, 2012; Abdul *et al.*, 2016; Yokoyama *et al.*, 2018). However, recent reviews of global fossil, coral-based sea-level data (e.g. Dutton & Lambeck, 2012; Medina-Elizalde, 2013; Hibbert *et al.*, 2016) have raised several key issues: (1) the bias towards high sea-level events (i.e. Holocene and MIS 5e highstands), (2) the lack of temporal coverage, particularly during interstadial/stadial and lowstand sea-levels, (3) a major bias towards co-seismically uplifted sites; and (4) ongoing debates about the reliability of the age determinations (Hibbert *et al.*, 2016; Chutcharavan *et al.*, 2018). Indeed, this is the case for MIS 3 where the precise timing, magnitude and rate of sea-level oscillation is still debated (see Siddall *et al.*, 2008 for reviews; Gowan *et al.*, 2021) in part due to the lack of appropriate absolute coral age data. Further, recent observations and models of Northern Hemisphere ice sheets (Pico *et al.*, 2018) suggest higher ESLs during MIS 3 than previously thought, while De Deckker *et al.* (2019) also argued for a rapid and steep drop in ESL, at least 100 mbsl, during MIS 4 between 71 and 59 ka.

Australia‘s North West Shelf (NWS) has a range of complex submerged submarine landscapes, including drowned platforms, terraces, banks, shoals, coastal barriers, dunes, tidal and estuarine channels (Anderson *et al.*, 2011; Brooke *et al.*, 2017; Moore *et al.*, 2017; O’Leary *et al.*, 2020) at depths of ~50 to 120 mbsl, making it an ideal natural laboratory to address these knowledge gaps (Fig. 1A). In recent years, extensive, industry 3D seismic surveys NW of Ashmore Reef have revealed much about the longer-term structural evolution of the margin, including insights about the major controls on distribution and growth of Miocene (Saqab & Bourget, 2016; McCaffrey *et al.*, 2020) and early Pleistocene (Saqab & Bourget, 2015) isolated carbonate build-ups (ICBs) that form the foundations of many of these banks. In parallel, there have been numerous biophysical surveys of the tops of these features, establishing their importance as recent and modern mesophotic reef habitats (Heyward, 1997; Heyward *et al.*, 2010; Anderson *et al.*, 2011). Sediment cores recovered from the adjacent shelf (i.e.

Bonaparte Gulf) have been used to reconstruct the history of MIS 2-deglacial RSL and associated sedimentary environmental changes (Nicholas *et al.*, 2014; Ishiwa *et al.*, 2016; Ishiwa *et al.*, 2019a). However, the lack of rotary drill cores from the adjacent submerged terraces, banks and shoals have left their ages and compositions unknown. Finally, this region of the NWS, directly adjacent to Timor-Leste, represents a key migration pathway for the first humans into Australia (Bird *et al.*, 2018; Fig. 1A). These migration models are based on assumptions that from ~70 to 10 ka, these platforms formed an emergent chain of habitable, resource-rich islands north-west (NW) of Australia. Again, the lack of absolute ages from those now submerged landscapes place uncertainties around palaeoenvironmental reconstructions and timing of occupation (O'Leary *et al.*, 2020).

Here, a unique suite of cores recovered from ~80 mbsl have been investigated as part of a geotechnical survey using a seabed rock drill (PROD) from the top of a drowned platform on the NWS ~150 km south-east (SE) of Ashmore Reef. The authors have combined available multibeam bathymetry and high-resolution 3D seismic data, along with detailed logging, high-resolution hyperspectral scanning, optical and scanning electron microscopy (SEM), sedimentary facies and palaeoenvironmental analyses using coralgal and larger benthic foraminifer assemblages and extensive ^{14}C-AMS and U/Th dating of the cores to: (1) characterise geomorphology of the platforms and adjacent shelf; (2) determine the internal chrono-stratigraphic evolution of the platforms, including succession of facies, mineralogical, diagenetic and palaeoenvironmental changes; (3) provide the first accurate constraints on MIS 3 reef growth and RSL in the region; and (4) discuss the development of the NWS reef and platform system in response to sea-level and associated palaeoenvironmental changes over the past 50,000 yr.

REGIONAL SETTING

The North West Shelf

The North West Shelf (NWS) is a ~2400 km-long physiographic feature (including the continental shelf, outer-shelf and marginal plateaus) located along the north-western margin of Australia that extends from Melville Island in the north-east to the Exmouth Gulf in the south-west (Bradshaw *et al.*, 1988; Purcell & Purcell, 1988; James *et al.*, 2004; Fig. 1A). The NWS includes four sedimentary basins (i.e. Northern Carnarvon, Roebuck, Browse, Bonaparte) and one orogenic belt (i.e. Timor-Banda Orogen; Longley *et al.*, 2002). The NWS experienced a complex tectono-stratigraphic evolution with periods of active rifting, collision and tectonic quiescence varying through time and space (Longley *et al.*, 2002; Marshall & Lang, 2013; Paumard *et al.*, 2018; Paumard *et al.*, 2019a).

The Bonaparte Basin (where the Ashmore Platform is situated) includes a series of Palaeozoic and Mesozoic depocentres and structural highs that developed during a multiphase tectonic history (Mory, 1991; Longley *et al.*, 2002; Marshall & Lang, 2013). In summary, the structural evolution of the Bonaparte Basin comprises: (1) two phases of Palaeozoic extension; (2) one phase of Late Triassic compression; (3) one phase of Mesozoic rifting followed by sea floor spreading; and (4) one phase of Neogene arc-continent collision (Bradshaw *et al.*, 1988; Gunn, 1988; Patillo & Nicholls, 1990; O'Brien *et al.*, 1993; O'Brien *et al.*, 1996; Shuster *et al.*, 1998; Cadman & Temple, 2004; Keep & Haig, 2010; Bourget *et al.*, 2012; Saqab *et al.*, 2017). Cenozoic sedimentation in the Bonaparte Basin evolved from a subtropical carbonate ramp to shallow-water, tropical carbonates

interrupted by brief periods of terrigenous siliciclastic inputs (Apthorpe, 1988; Mory, 1991; Whittam *et al.*, 1996; Longley *et al.*, 2002; Saqab & Bourget, 2016).

Although located at similar latitude to the central and northern Great Barrier Reef (GBR), modern NWS reefs are far less extensive, consisting of series of relatively small isolated shelf edge pinnacle and atoll reefs and inshore fringing reefs (Kordi & O'Leary, 2016). These shelf edge reefs represent the remnants of an extensive Miocene 'Great Barrier Reef' extending from near the equator to 22°S that drowned due to subsidence in the late Miocene (McCaffrey *et al.*, 2020). Last Interglacial (LIG) reefs have been observed on the NWS at Cockatoo Island at a depth of 16 m below the modern fringing reef platform (Solihuddin *et al.*, 2015) and seismically inferred at a depth of 25 m below the modern reef platform on mid-shelf Adele Reef (Solihuddin *et al.*, 2016). These observations, combined with the depth (~26 m) and age of the LIG reef below the modern Scott Reef, suggest that the NWS experienced significant Late Pleistocene subsidence at rates on the order of ~0.2 to 0.45 mm yr^{-1} (Collins *et al.*, 2011; Solihuddin *et al.*, 2016). This is an order of magnitude faster than the Neogene continental-scale subsidence of the northern margin of Australia estimated by Sandiford (2007) at 15 to 20 m myr^{-1}.

Oceanography and climate

At 12°S the Ashmore Platform is on the southerly edge of the West Pacific Warm Pool (WPWP) (Fig. 1) just north of the 28° C sea-surface temperature (SST) isotherm (Gallagher *et al.*, 2009; Rosenthal *et al.*, 2018) downstream of the Indonesian Throughflow (ITF; Gordon, 2005; Gallagher *et al.*, 2017). The ITF is a major arm of the global thermohaline circulation that transports warm waters from the Pacific Ocean into the Indian Ocean, exerting a major control on the distribution of reefs in the eastern margin of the Indian Ocean (Gallagher *et al.*, 2014).

The arid to semi-arid climate of the Australian interior extends to the north-west coast of Australia. To the north, rainfall is variable yet mainly monsoonal, with the dominance of summer rainfall declining sharply towards the south (Sturman & Tapper, 2005). Warm, moist, equatorial air is the major source of monsoonal and cyclonic rain in the north but it is replaced in the south by tropical air from the Indian Ocean also known as the 'pseudo-monsoon' (Gentilli, 1972). During the Austral summer, north-westerly winds bring monsoonal rains (Australian Summer Monsoon – ASM) to the Kimberley region, whereas atmospheric circulation changes in the dry season (Austral winter) bringing south-easterly trade winds and dust from the arid Australian interior.

MATERIALS AND METHODS

Sample sites, bathymetry and seismic data

A recent compilation of available source bathymetry data off northern Australia into a ~100 m pixel digital elevation model (DEM), called the nthaus100 grid (Beaman, 2018), with a $\pm$~2.5 m vertical uncertainty, shows that the drill sites are on a north-west to south-east trending platform near Ashmore Reef in variable water depths from 90 to 50 mbsl (Fig. 1A). Industry 3D seismic surveys, Onnia-1 and Onnia-2, were accessed through Geoscience Australia and provided a high-resolution, spatially contiguous bathymetric dataset covering the Ashmore Platform, with a bin spacing (i.e. spatial resolution) of 12.5 x 12.5 m, for an average vertical resolution of ~15 to 20 m across the study area. Three high-resolution (5 m) multibeam passes across the platform, also included in the nthaus100 grid, provide additional depth ($\pm$~1 m) constraints (Fig. 2) on the geomorphic features described in

section 4.1. Following the methodology detailed by Paumard *et al.* (2019b) and O'Leary *et al.* (2020), the PaleoScan™ sea floor digital elevation model was imported and merged into ArcGIS including ArcMap software for shaded relief/slope analysis that allowed interpretation of the sea floor geomorphology of the region (Fig. 2). The detailed sea floor morphology covers an extensive area of the drowned platforms and surrounding shelf. This map is resolved at much higher resolution compared with the generally sparse bathymetry data available in the region within the nthaus100 grid, which does not include the 3D seismic-derived bathymetry data.

Fig. 3 shows the location of the drill site transects and a comparison of the spatial resolution between the nthaus100 bathymetry (Fig. 3A) and 3D seismic-derived bathymetry (Fig. 3B). The SW transect occupies a more exposed position on the platform(s) compared with the NW transect, based on comparison with modern regional oceanographic conditions (including Ashmore Reef) and the dominant south and south-easterly winds and waves (Berry, 1993; Glenn & Collins, 2005).

Seabed drilling operations and core recovery

Cores were collected between 2006 and 2007 using a seabed drilling system (PROD) as part of a geotechnical survey conducted by PTTEP (PTT Exploration and Production Public Company Limited) Australasia (Fig. 2B). The survey cored and/or penetrated 21 holes from 13 sites along two transects (NW and SW) between 74 and 98 mbsl (Fig. 2) with a maximum penetration of 28 m (Table 1). The drill site water depths, and subsequent sample depths, are not corrected for tide or to any particular datum. However, the maximal tidal range uncertainty ($\pm$ 0.9 to 2 m) was applied for each site based on the day the site was drilled using hindcast tidal predictions from the closest tidal station (AusTides Skua No.4 - Australian_Hydrographic_Office, 2018).

Not all holes were continuously cored; others were subjected to cone penetrometer testing (denoted with the sample suffix 'C'; Table 1) and some recovered sections were unavailable due to subsequent geotechnical testing. This study focusses on 10 holes from 7 sites that had the deepest penetration and highest recoveries from the NW and SW transects (Table 1). Total average core recovery was ~25% including all missing sections (i.e. non-sampled sections, *in situ* cone penetrometer testing and geotechnical testing). However, in this study the authors have focussed their analyses on the most complete holes with commonly > 85% recovery and where the core quality was excellent. Any missing and non-sampled intervals of the core are labelled as 'missing' and indicated on the stratigraphic logs.

Stratigraphic, sedimentary facies and reef assemblage analysis

Cores were logged using a combination of physical core material, computed tomography (CT) scans and petrographic thin sections using established criteria (Abbey *et al.*, 2011; Dechnik *et al.*, 2015; Humblet & Webster, 2017). Four distinct chrono-stratigraphic units and their boundaries were defined, based on major changes in sedimentary facies, biotic assemblages, macro and micro mineralogical and diagenetic characteristics (thin section petrology, scanning electron microscope [SEM], hyperspectral imagery) and available radiometric dating information (details below).

Ten sedimentary facies were identified based on primary framework and detrital fractions following established criteria (Camoin *et al.*, 2007; Dechnik *et al.*, 2015; Table 2; Fig. 4). Corals were identified to generic level or species, where possible, in

well-preserved samples based on modern and fossil taxonomic guides (Veron & Wallace, 1984; Wallace, 1999; Veron, 2000; Budd *et al.*, 2012; Huang *et al.*, 2014; Humblet *et al.*, 2015; Huang *et al.*, 2016; Richards, 2016) (Table 3). Sixty thin sections were used to identify the taxonomic composition of crustose coralline algae (CCA) and larger benthic foraminifers (LBF; Renema, 2010; Renema, 2018; Table 3) and their main assemblages (Table 4). The taxonomic approach and palaeoenvironmental interpretation based on CCA follows the procedure indicated in Humblet *et al.* (2019).

The abundance of vermetid gastropods was tallied into three categories (category 3 = >10, category 2 = 5 to 10 and category 1 = 0 to 5 vermetid individuals per CCA crust) following Dechnik *et al.*, (2017). Coralgal assemblages were defined on the basis of the dominant coral, CCA and LBF types, vermetid gastropod abundance and comparisons with modern depositional environments from Western Australian and the wider Indo-Pacific (see below for supporting references) (Table 4).

Radiometric dating, XRD, SEM and hyperspectral mineralogical analysis

Coral, coralline algal and mollusc samples were chosen from the best preserved sections of the NWS cores for ^{14}C-AMS and U/Th dating. Care was taken to select samples free of obvious diagenetic alteration (e.g. dissolution, staining, sediment fill, minimal secondary cement). Furthermore, thin section petrology, SEM, XRD and hyperspectral data were also used to evaluate the reliability of the resulting ages following recognised methodologies (e.g. Sanborn *et al.*, 2020). Limited reconnaissance ^{14}C dating of a stratigraphically deeper and clearly diagenetically different reef unit was undertaken to confirm that it is older than the radiocarbon dating window (e.g. ~50 ka BP; Stuiver *et al.*, 2020).

All samples for ^{14}C-AMS dating were ultrasonically cleaned in continuously replaced Nano-pure water. The powdered coral, coralline algal and mollusc samples (1 to 2 mg) were prepared using the small-volume graphitisation vacuum line and measured by accelerator mass spectrometry (AMS) at the Analytical Center for Environmental Science, Atmosphere and Ocean Research Institute, University of Tokyo, Japan (Yokoyama *et al.*, 2010; Hirabayashi *et al.*, 2017). All of the radiocarbon dated samples reported herein have undergone a severe acid leach, approximately discarding 30 to 40% of each sample aliquot (Yokoyama *et al.*, 2000; Yokoyama *et al.*, 2007). The ^{14}C ages were converted to calendar ages (ka) with 2σ errors using CALIB.8.1.0 and the Marine20 international calibration datasets (Stuiver *et al.*, 2020), with a weighted mean Delta-R (ΔR) value of 64 ± 39 ^{14}C yr based on the four nearest points (<500 km apart) (Table 5).

Three paired U-Th coral ages were produced at The University of Queensland Radiogenic Isotope Facility (RIF; Table 6 for complete isotope data). Subsamples (~1 g) were taken from corals representing *in situ* growth, then cleaned in an ultrasonic bath. Subsamples were crushed into ~1 mm chips, which were soaked for 24 h in a 15% H_2O_2 solution, sonicated for 15 min and rinsed in milliQ water three times before being dried on a hotplate at 60° C overnight. After this pre-treatment, 0.15 g of the most pristine aragonite fragments were hand selected under optical microscope to be included in U-Th geochemical analysis. Prior to analysis, subsamples were digested in double-distilled HNO_3 and a ^{229}Th-^{233}U mixed tracer was used to spike samples. The three ages were measured in duplicate on a Nu Plasma HRMulti-Collector-Inductively Coupled Plasma-Mass Spectrometer (MC-ICP-MS) in 2019. Details of sample vetting, U-Th geochemical procedures, initial ^{230}Th

corrections and age calculations follow Zhao *et al.* (2009), Clark *et al.* (2014) and Salas-Saavedra *et al.* (2018). Ages were calculated using the program Isoplot 3.75 (Ludwig, 2012) utilising decay constants of Cheng *et al.* (2000). All ages were converted into years BP (relative to 1950) for comparison with ^{14}C dates (Table 5) and are presented in ka BP in this study.

SEM analysis was performed on representative dated coral, coralline algae and mollusc samples using a Hitachi Tabletop SEM at Queensland University of Technology (QUT) (TM3000) and Wenona School (Sydney) (TM4000). Samples were examined to confirm the absence of significant secondary cements, boring, staining, dissolution, recrystallisation and sediment fill (Nothdurft & Webb, 2009; Salas-Saavedra *et al.*, 2018), whilst providing a comprehensive description and catalogue of main diagenetic features and environments (marine, meteoric) observed down hole (Braithwaite & Montaggioni, 2009; Gischler *et al.*, 2013).

With two exceptions, XRD analysis was undertaken on all ^{14}C-AMS and U/Th dated corals to test for low-Mg calcite. Samples ~1 g were hand ground to a powder in an agate mortar and pestle under ethanol. Samples were front-pressed into circular quartz sample holders. Powder X-ray diffraction patterns were acquired using a Malvern PANalytical X'Pert Pro Powder X-ray diffractometer using a cobalt tube (40 kV, 40 mA) in Bragg-Brentano geometry. Patterns were collected over 1 hr from 5 to 90 °2θ at a step size of 0.0167°. Incident optics included 0.04 rad Soller slits, 15 mm mask, 1° anti-scatter slit and 0.25° fixed divergence slit. Receiving optics before the X'Celerator detector were 0.04 rad Soller slits, an Fe kβ filter and a 5.0 mm anti-scatter slit. Samples were spun during data collection at a speed of 2 rps. Rietveld refinement was performed in TOPAS (V5, Bruker). An instrument response function previously determined from NIST SRM660A was used to model kβ radiation and the intrinsic peak shape. Refined parameters included 15 term Chebyshev background, scale factors and unit cell parameters for each phase, specimen displacement and a Lorentzian crystallite size term to account for peak broadening for each phase.

High-resolution (~0.33 mm per square image pixel) hyperspectral data were also acquired in the shortwave infrared (980 to 2500 nm) from 74 representative core sections to map and quantify mineralogic and lithological variations, along with amounts of hydroxyl (OH) and H_2O. Classified images of carbonate (aragonite, calcite and dolomite) were derived using the method of Murphy *et al.* (2017). The shape of primary carbonate absorption at ~2331 nm was used as an indicator to detect subtle changes in carbonate mineralogy across the core sections. The shape of the feature was quantified in terms of its wavelength position, intensity and asymmetry. With increasing intensity of diagenesis and alteration of aragonite to calcite, the shape of the ~2331 nm carbonate absorption changes, specifically: i) wavelength position shifts to longer wavelengths, ii) intensity increases; and iii) the feature becomes more left-asymmetric (as indicated by increasingly negative asymmetry values). Purity or crystallinity of calcite in the sections was quantified as the area of minor (secondary) carbonate absorption at ~1880 nm, which is present only in pure or crystalline calcite. Its area is proportional to the purity/crystallinity of the calcite in the section. The amount of OH and H_2O was quantified as the area of the primary OH and H_2O absorptions at ~1430 and 1930 nm, using the method described by Murphy *et al.* (2021).

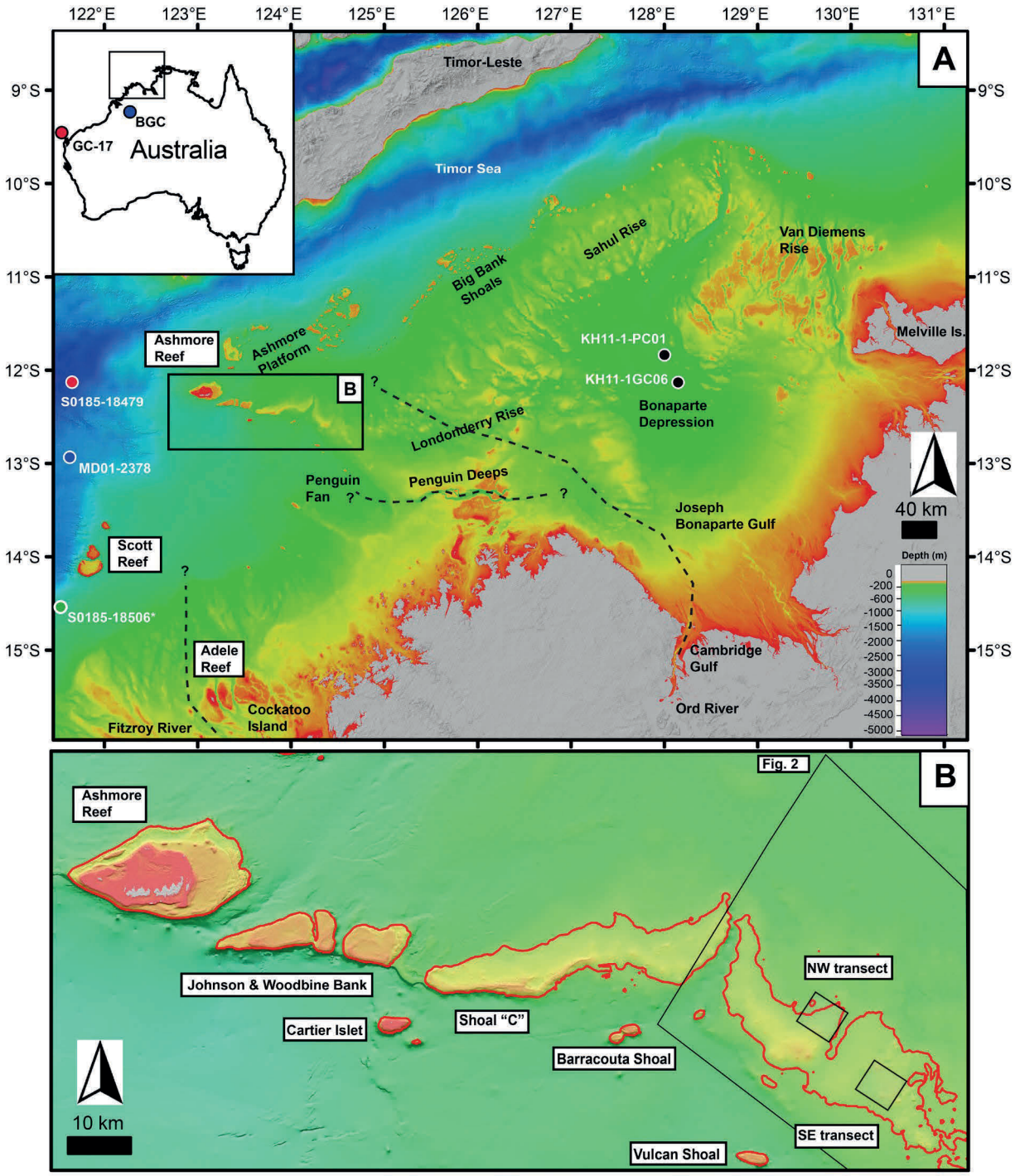

Fig 1. (A) Regional topography and bathymetry map (100 m DEM) showing the location of the main study sites and other locations (marine sediments cores, speleothems) referred to in the study (bathymetry data: Beaman, 2018). The black dash lines represent the interpreted position of the palaeo-Fitzroy and Ord rivers on the NWS during lower sea-levels (after Glenn, 2004; Kuhnt *et al*., 2015). (B) Close-up map showing the geomorphology of the Ashmore platform structure and the location of the NW and SW coring transects (black squares). The larger black polygon represents the wider area shown in Fig. 2 that also incorporates the 3D seismic-derived seabed geomorphology data. The red line represents the -80 m depth contour from the nthaus100 grid.

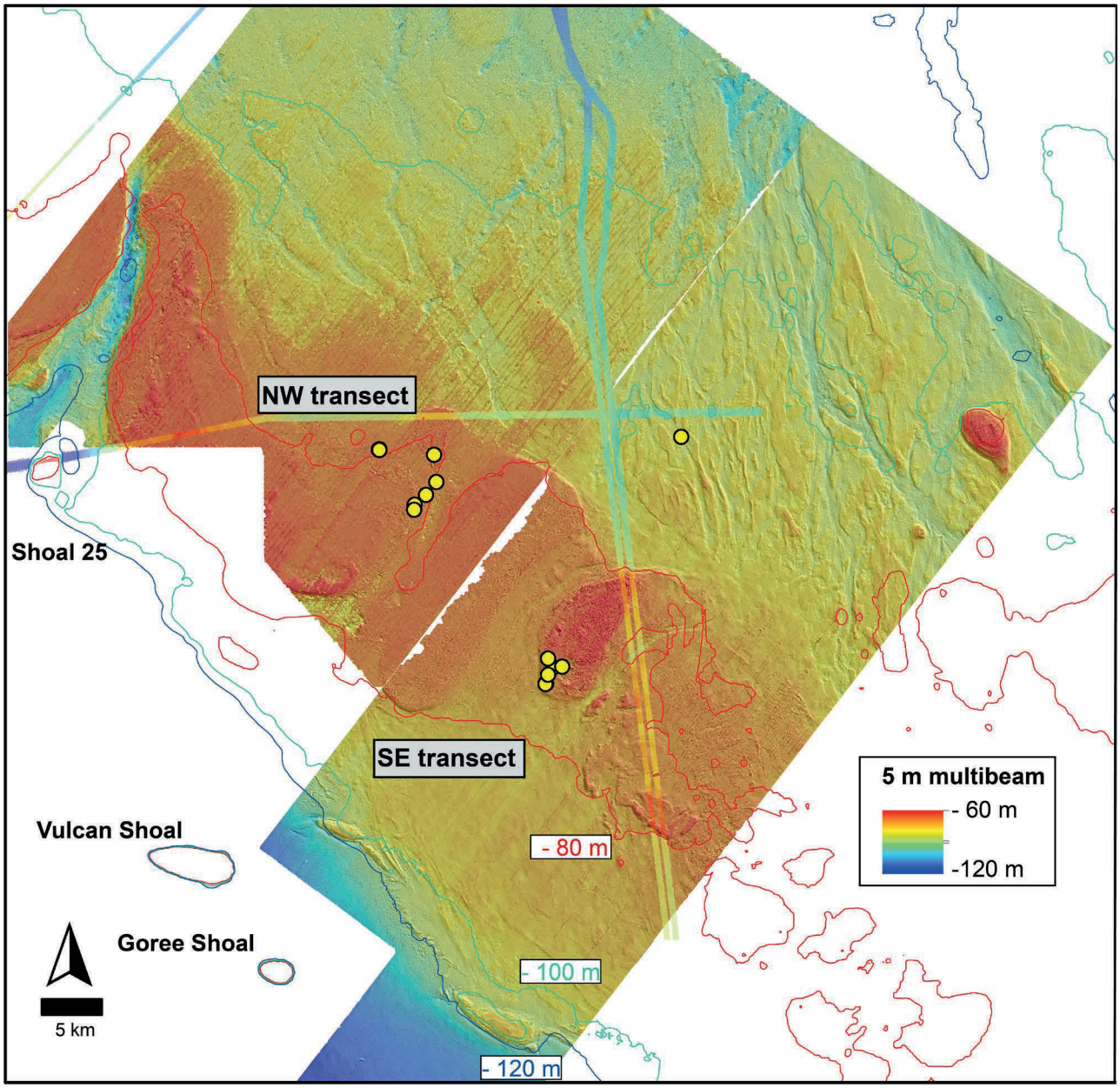

Fig 2. 3D seismic derived seabed geomorphic map of the platform and adjacent region. The limited 5 m gridded multibeam data are also shown.

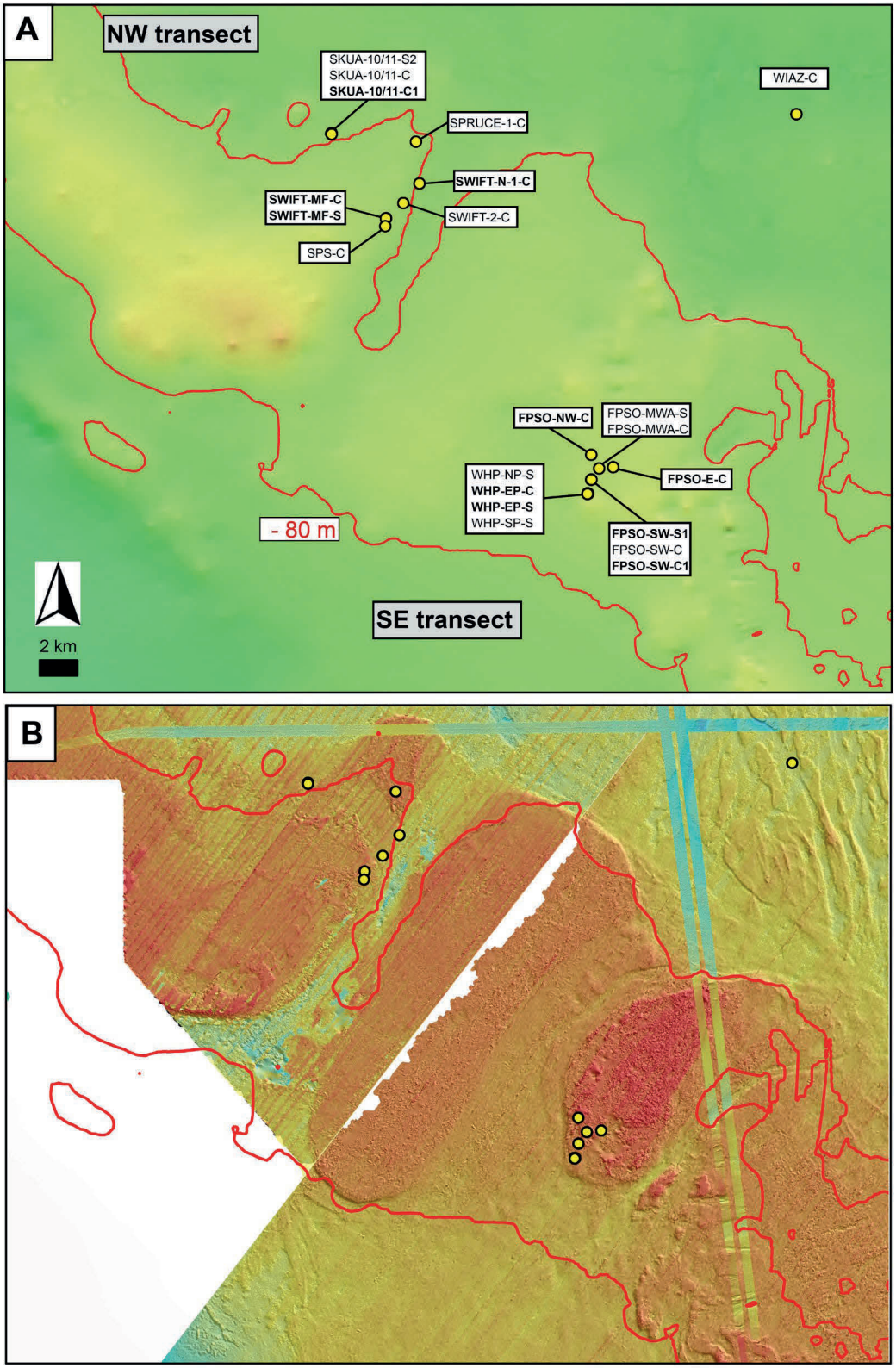

Fig 3. Close-up maps showing NWS core locations forming NW and SW transects. The red line represents the -80 m depth contour. (A) nthaus100 bathymetric grid (Beaman, 2018). (B) 3D seismic-derived bathymetry.

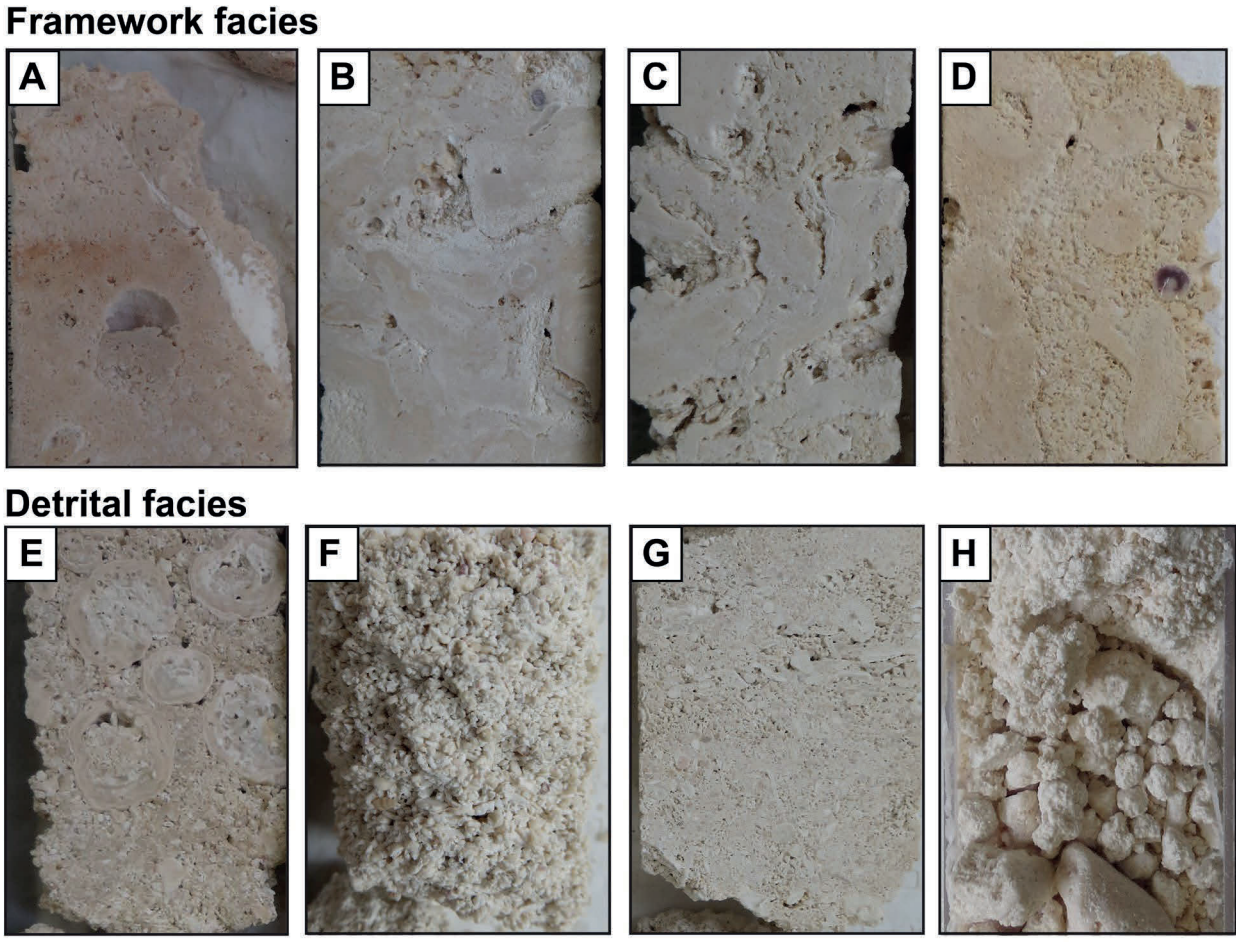

Fig 4. Main lithologies in NWS cores divided into framework and detrital facies. (A) Framestone, massive coral-dominated (SWIFT-N-1-C-2BB1). (B) Framestone, submassive-encrusting coral-dominated (WHP-EP-C-3A). (C) Bindstone, encrusting coralline algal-dominated (FPSO-NW-C-7B). (D) Bafflestone, branching coral-dominated (FPSO-NW-C-1A). (E) Floatstone, rhodolith-dominated (FPSO-NW-C-6A). (F) Grainstone, larger benthic foraminifera-dominated (WHP-EP-C-9A). (G) Packstone-grainstone, larger benthic foraminifera and coralline algal-dominated (WHP-EP-C-7BB1). (H) Unconsolidated coral rubble and carbonate sand (WHP-EP-S-11A). Core diameter is 4.5 cm in all images.

Table 1. Summary of NWS drill site locations and metadata.

Site[a]	Tran-sect	Date	Easting (m)[b]	Northing (m)	Seabed water depth (mbsl)[c]	Tide error +/- (m)[c]	Hole penetr-ation (m)	Total recovered core (m)[d]	Hole penetr-ation (mbsl)
SKUA-10/11-C	NW	29/03/03	654054.99	8617597.95	79.6	1.2	9.6	0.9	89.2
SKUA-10/11-C1	NW	7/04/03	654083.56	8617628.49	81.6	1.6	10.6	2.6	92.2
SKUA-10/11-S2	NW	7/04/03	654080.47	8617576.78	78	1.6	4.4	0.2	82.4
SPRUCE-1-C	NW	29/03/03	658427.9	8617155.61	76.5	1.2	10.5	3.0	87.0
SWIFT-N-1-C	NW	30/03/03	658604.2	8614952.19	81.5	1.4	10.3	3.5	91.8
SWIFT-2-C	NW	8/04/02	657766.92	8613925.37	80.1	0.9	11	2.3	91.1
SWIFT-MF-C	NW	30/03/03	656869.85	8613135.87	78.5	1.4	12.2	2.7	90.7
SWIFT-MF-S	NW	30/03/03	656863.62	8613130.78	76.4	1.4	2.6	0.9	79.0
SPS-C	NW	8/04/03	656825.26	8612726.39	78.3	1.4	10.7	3.1	89.0
WHP-EP-C	SW	31/03/03	667216.09	8598605.28	78.5	1.6	27.15	2.6	105.7
WHP-EP-S	SW	4/04/03	667216.99	8598602	78.2	2.0	27.8	7.1	106.0
WHP-NP-S	SW	5/04/03	667188.09	8598617.69	77.3	1.9	0.6	0.0	77.9
WHP-SP-S	SW	5/04/03	667185.08	8598583.11	78	1.9	0.6	0.0	78.6
FPSO-SW-C1	SW	5/04/03	667380.2	8599333.43	77.3	1.9	22.7	4.6	100.0
FPSO-SW-S1	SW	8/04/02	667385.61	8599336.51	78	0.9	21.3	6.8	99.3
FPSO-SW-C	SW	31/03/03	667380.51	8599337.04	76.7	1.6	0.7	0.0	77.4
FPSO-NW-C	SW	7/04/03	667382.67	8600640.76	78.9	1.6	21.5	4.4	100.4
FPSO-E-C	SW	6/04/03	668511.45	8599985.35	74.8	1.8	21.4	6.1	96.2
FPSO-MWA-C	SW	5/04/03	667792.49	8559927.21	78.6	1.9	10.4	2.9	89.0
FPSO-MWA-S	SW	5/04/03	667791.61	8599922.74	75.9	1.9	0.8	0.0	76.7
WIAZ-C		9/04/02	678082.68	8618484.87	97.5	1.1	11.8	0.0	109.3

[a]Drill sites highlighted in bold are focus of this study. Sites in adjacent rows (e.g. SWIFT-MF-C, SWIFT-MF-F) represent replicate sites given their proximity. Some holes were not continuously cored and were subjected to cone penetrometer testing (denoted with sample sufix code 'C'.

[b]Datum: Geocentric Datum Australia 1994 (GDA94); Coordinates transformed from ITRF2000 to GDA94 Datum using 7-parameter transformation values (Epoch 2007.5). Projection: Map Grid Australia Zone 51, CM 123 degrees East.

[c]Depths are water depths below sea-level (mbsl) of the PROD landing on the seabed and are not corrected for tide or to any particular datum. However, the authors apply the maximum tidal range uncertainty for each site based on the day the site was drilled using hindcast tidal predictions from AusTides Skua No.4 (Australian Hydrographic Office, 2018).

**C= Cone Penetrometer Testing, S =Sampling.

[d]Estimated total recovered core for each site accounting for missing sections (non-sampled sections, *in situ* cone penetrometer testing and further geotechnical testing).

Table 2. Main sedimentary facies observed in the NWS cores.

Facies	Dominant components
Framework facies	
Framestone	*In-situ* coral framework sometimes associated with coralline algal crusts.
Bindstone	Thick coralline algal crusts (>10 mm) commonly binding *in-situ* corals. Vermetid gastropods common.
Bafflestone	Branching coral framework, autochthonously binding grainstone/ packstone sediments between branches.
Detrital facies	
Floatstone	Grainstone/packstone supported matrix with >10% composed of coralline algal, shell & coral fragments >2 mm.
Rhodolith floatstone	Grainstone/packstone supported matrix with ~20 to 40% composed of coralline algal rhodoliths 5 to 20 mm in diameter.
Mollusc floatstone	Grainstone/packstone supported matrix with ~20 to 40% composed of mollusc & gastropod shell fragments >2 mm.
Grainstone	Semi-lithified, grain-supported sediments composed of mainly of larger benthic foraminifera (LBF) with mollusc shell & coral fragment.
Grainstone/ packstone	As above but with ~10 to 20% lime mud in the matrix.
Wackestone	Mud supported with <20% sand sized sediments, with few (<10%) coral fragments.
Coral rubble	Unconsolidated coral clasts sometimes associated with a packstone matrix.

Table 3. Summary of the coral, coralline algal and large benthic foraminifera taxa observed in the NWS cores.

Corals	**Coralline algae**	**Large benthic foraminifera**
Family	Order	Family
ACROPORIDAE	**CORALLINALES**	**NUMMULITIDAE**
Acropora sp.	*Porolithon* gr. *onkodes*	*Heterostegina depressa*
Acropora gr. 21 (*A.humilis*, *A.gemmifera, A. monticulosa) Acropora* gr. 22 (*A. digitifera*)	*Porolithon gardineri* *Amphiroa* sp. *Dawsoniolithon conicum*	*Cycloclypeus carpenteri* *Operculina* sp. (*ammonoides* group)
Acropora gr. 25 *Acropora* gr. 26 (*A. aspera?*)	*Dawsoniolithon* sp. *Harveylithon* gr. *munitum*	Family **CALCARINIDAE**
Acropora gr. 27 (*A. latistella*) *Isopora palifera*	*Harveylithon* gr. *rupestre* *Harveylithon* sp.	*Neorotalia calcar*
Montipora gr. 9 (*M. hispida*?) *Montipora* sp. (encrusting-submassive)	*Hydrolithon boergesenii* *Hydrolithon* sp. *Lithophyllum* gr. *acrocamptum*	*Calcarina hispida* gr. *Calcarina spengleri* *Calcarina mayori*
Family **MERULINIDAE**	*Lithophyllum* gr. *kotschyanum Lithophyllum* gr. *prototypum* *Lithophyllum* gr. *pustulatum*	*Calcarina* indet. *Schlumbergerella floresiana*
Goniastrea gr. 1 *Platygyra sinensis?*	*Lithophyllum* sp. *Neogoniolithon* spp.	Family **AMPHISTEGINIDAE**
Dipsastraea gr. 1 (*D. stelligera*?) *Dipsastraea* gr. 2	Order **HAPALIDIALES**	*Amphistegina lobifera* *Amphistegina lessonii*
Favites gr. 1		*Amphistegina radiata*
Cyphastrea sp.	*Lithothamnion* gr. *proliferum*	
Echinopora sp.	*Lithothamnion* spp.	Family **SORITIDAE**

Family **AGARICIDAE**

Pavona clavus

Pavona explanulata

Family **POCILLOPORIDAE**

Stylophora pistillata

Seriatopora sp.

Family **PORITIDAE**

Goniopora gr. 4

Porites gr. 1 (*P. lutea, P. australensis*?)

Porites gr. 6 (*P. cylindrica, P. nigrescens*)

Porites gr. 4/5

Family **MILLEPORIDAE**

Millepora sp.

Order **SPOROLITHALES**

Sporolithon sp.

Other red algae

Peyssonnelia spp.

Amphisorus sp. 1 (thin)

Amphisorus sp. 2 (thick)

Sorites sp.

Family **PENEROPLIDAE**

Peneroplis cf planatus

Family **ALVEOLINIDAE**

Alveolinella quoyi

Borelis sp.

Other Foraminifera

Sphaerogypsina globulus

Elphidium craticulatum

Table 4. Summary of coral, coralline algal and large benthic foraminifera assemblages in the NWS cores and their probable palaeoenvironmental settings.

Assemblage	Main components	Associated biota	Palaeoenvironmental interpretation
Coralline algae (CCA)			
A1	Thick crusts of *Porolithon* gr. *onkodes*		Shallow, high energy reef settings, 0 to 10 m
A2	*Lithophyllum* spp. (*L.* gr. *kotschyanum, L. gr. acrocamptum*, and *L* gr. *pustulatum*) with associated *Harveylithon* spp. (*H.* gr. *munitum* and *H. gr. rupestre*)		Intermediate reef slope settings, 0 to 30 m
A3	Laminar *Lithothamnion* spp, with associated thin crusts of *Lithophyllum* gr. *pustulatum, Lithoporella* and *Peyssonnelia*		Deeper reef slope, >20 m
Larger benthic foraminifera (LBF)			
LBF1	*Schlumbergerella* sp. and *Amphistegina lobifera* with associated *Amphisorus* sp, *Calcarina hispida*, and *Peneroplis* sp.		Reef crest and flat settings 0 to 10 m
LBF2	*Amphistegina radiata* and *Heterostegina depressa* with associated *Calcarina spengleri* and *Alveolinella quoyi*		Reef slope settings, 5 to 50 m
Coralgal			
C1	*Acropora* (*A. humilis, gemmifera, monticulosa*) (robust corymbose/digitate branching), *Stylophora pistillata* and branching *Porites* (*P. cylindrica, P. nigrescens*), with associated *Isopora palifera* and *Montipora* (sub-massive/encrusting)	A1, LBF1, V3-2	Shallow, very high energy, reef crest-upper slope settings, 0 to 10 m; 0 to 5 m*
C2	*Acropora* (corymbose branching, partially dissolved) and merulinids (*Dipsastraea* gr. 2), with associated *Montipora* (encrusting-sub-massive) and *Seriatopora* (branching)	A2, V1-2	Intermediate reef slope settings, 0 to 30 m
C3	*Acropora* (digitate & robust corymbose branching) and *Porites* gr. 1 (massive)		Shallow, high energy, reef settings, 0 to 10 m

	with associated merulinids *(Dipsastraea* gr. 1)	A1, LBF1, V2	
C4	*Pavona clavus* (columnar), with associated *Acropora* (digitate), *Montipora* (columnar/encrusting), *Pocillopora* (branching) and *Pavona explanulata* (thin encrusting)	A2, LBF1?	Intermediate depth and energy, sheltered back reef settings, >10 to 30 m

RESULTS

Platform and shelf geomorphology

The 3D seismic-derived bathymetry map, with available high-resolution multibeam, reveals extensive new details about the geomorphology of the platform top and surrounding shelf to the NE and SW (Figs 2 and 3). Rather than forming a single continuous platform, the Ashmore Platform is divided into at least three distinct NE/SW trending, oval shaped platforms as much as 22 km-long and 26 km-across, in places rising ~30 m above the surrounding sea floor to ~60 mbsl and separated by channels as deep as ~120 mbsl (Fig. 3B).

Rising from greater than ~95 mbsl, the platforms are rimmed by a series of small but distinct terraces that can be traced continuously as much as 20 km at ~90 mbsl, 80 mbsl, 70 mbsl and a shallowest terrace ~60 mbsl limited to the SE margin. The drill sites are located on the widest 80 m terrace, with the SE transect (FPSO, WHP) located on the seaward edge of the platform, while the NW transect (SWIFT, SKUA) is situated ~10 km back from the seaward SE edge of the larger platform but proximal to the dividing channel (Fig. 3A and B). SE of the platform complex, the sea floor is relatively smooth until ~95 m where it is marked by a succession of ~10 en echelon, linear to arcuate, NW-SE trending ridges down to ~110 m that are ~100 to 300 m-wide and ~400 to 800 m-apart. Just seaward of these ridges are two smaller (4 to 8 km) oval shaped platforms that are rimmed by at least four smaller terraces between ~120 and 100 mbsl. While the tops of these platforms are in deeper water (~90 to 100 mbsl), they are similar in shape to a series of submerged oceanic banks and shoals farther to the SW (e.g. Shoal C, Barracouta shoal, Vulcan shoal, Shoal 25). The Vulcan Shoal, only 8 km away, rises to ~20 to 30 mbsl but also has a distinct step or terrace at ~80 mbsl (Moore *et al.*, 2017; Figs 1B and 2B). In contrast, the shelf geomorphology NE of the main - 80 m platforms and drill transects is distinctly different. There, the sea floor between ~90 and 110 mbsl is characterised by a complex network of NNW trending channels and elongate bank features (~8 to 10 m channel depths) and by the distinct absence of narrow meandering channel or oxbow lake morphologies.

Biologic assemblages and palaeo-environmental settings

Coralline algal assemblages (CCA)

Three distinct coralline algal assemblages (Table 4, Fig. 5) were established in the NWS cores, based on dominant algal genera and, where possible, species. Based on comparisons with their modern CCA counterparts and previously established fossil assemblages from the Indo-Pacific, there are three different palaeoenvironments, ranging from shallow, high-energy (<6 to 10 m), intermediate (0 to 30 m) and definitively deeper reef slope settings (>20 m).

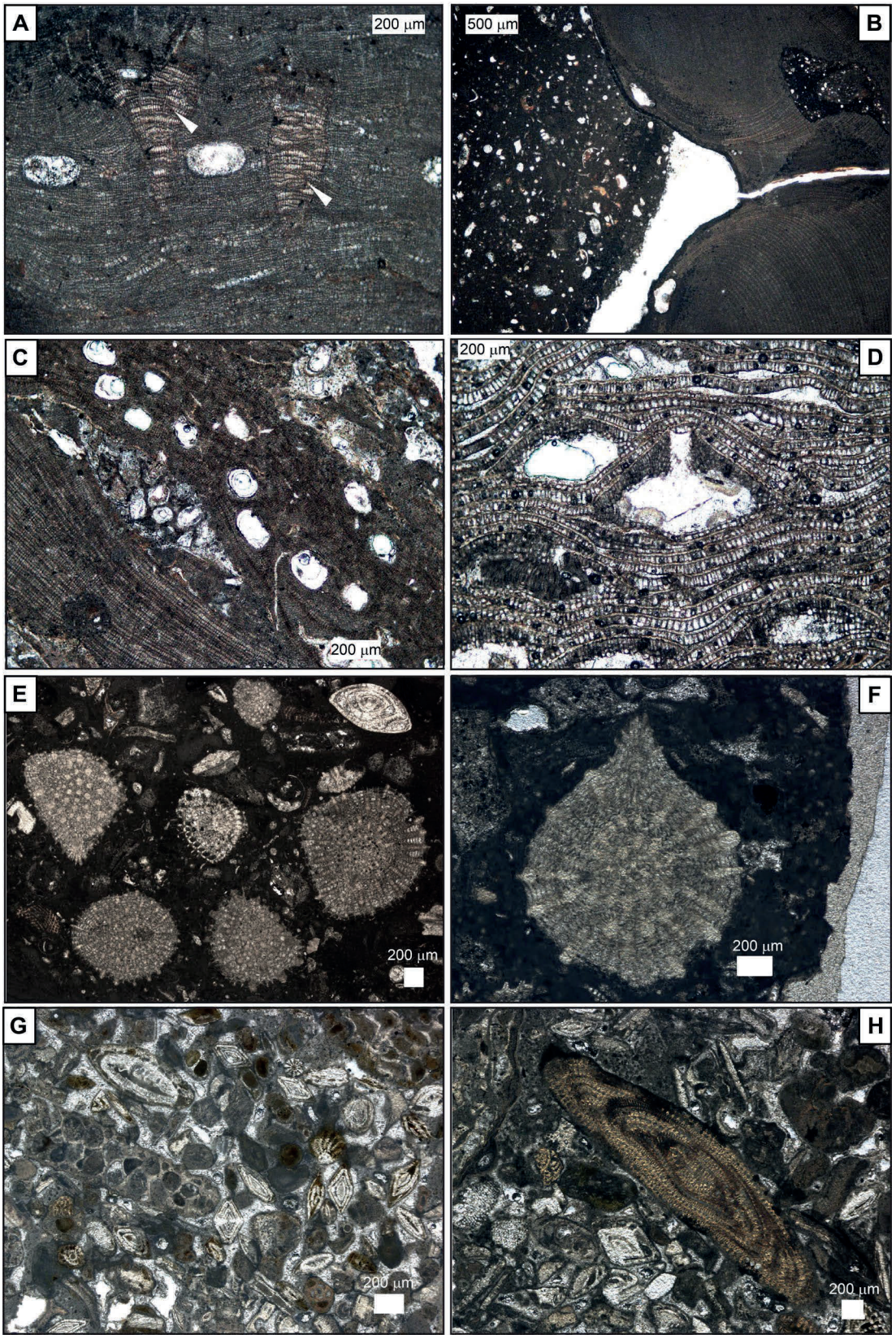

Fig. 5. Thin section images showing the main coralline algal (CCA) and benthic foraminifera assemblages (LBF) in NWS cores. (A) Crust of *Porolithon* gr. *onkodes* with two semi endophytic thalli of *Lithophyllum*

gr. *cuneatum* (white arrow heads) that are characteristic of shallow-water settings (A1 assemblage) (WHP-EP-C-3A). (B) Branches of *Lithophyllum* gr. *kotschyanum* with conceptacles (FPSO-EC-1A); and (C) a crust of Hapalidalean CCA with many conceptacles growing on a *Lithophyllum* crust (bottom left); both are common in shallow to intermediate waters (A2 assemblage) (SWIFT-N1-C-1A). (D) Crust of superimposed applanate branches of *Lithoporella*, typical of deep-water settings (or darkened sites), showing two conceptacles (A3 assemblage) (FPSO-SW-C1-1A). (E) Overview of the *Schlumbergerella floresiana*-dominated assemblage with associated *Amphistegina* spp. (right top corner) typical of shallow-water reef and platform top settings (LBF1 assemblage) (FPSO-EC-1A). (F) Close up showing *Schlumbergerella floresiana* (LBF1 assemblage) (WHP-EP-S-3A). (G) Overview showing *Amphistegina radiata*-dominated assemblage (with *Heterostegina depressa* & a textularid) typical of deeper reef slope settings (LBF2 assemblage) (SKUA-10-11-C1-5A). (H) Close up showing details of the *Amphistegina* spp. assemblage with *Alveolinella quoyi* and *Calcarina* spp. (LBF2 assemblage) (WHP-EP-S-15A).

Algal Assemblage 1 (A1) is dominated by thick, centimetre-scale crusts of *Porolithon* gr. *onkodes* with associated semi-endophytic *Lithophyllum* gr. *cuneatum* (Fig. 5A), thin crusts of *Lithophyllum* gr. *pustulatum* and scattered *Lithophyllum* gr. *prototypum* and *Harveylithon* spp. Living *P.* gr. *onkodes* is common in shallow-water (<10 m), high-energy environments throughout the Indo-Pacific (Adey *et al.*, 1982; Verheij, 1994; Iryu *et al.*, 1995; Cabioch *et al.*, 1999; Payri *et al.*, 2000; Dechnik *et al.*, 2017; Braga *et al.*, 2022). Analogous fossil assemblages dominated by *P.* gr. *onkodes* are similarly characteristic of shallow reef settings in palaeowater depths of <10 m and <6 m where associated with thick algal crusts and abundant vermetid gastropods (Cabioch *et al.*, 1999; Abbey *et al.*, 2011; Camoin *et al.*, 2012; Gischler *et al.*, 2016; Dechnik *et al.*, 2017; Humblet *et al.*, 2019).

Algal Assemblage 2 (A2) is dominated by *Lithophyllum* species (*L.* gr. *kotschyanum, L.* gr. *acrocamptum* and *L.* gr. *pustulatum*) with associated *Harveylithon* (*H.* gr. *munitum* and *H.* gr. *rupestre*) with thin (<0.2 mm) crusts of *Hydrolithon* sp. and minor Hapalidiales (Fig. 5B and C). This assemblage commonly comprises the crusts forming the rhodolith-dominated facies. Fossil assemblages dominated by *Lithophyllum* and *Harveylithon* species with no crusts of *P.* gr. *onkodes* typically occur in shallow to intermediate depths to 30 m throughout the Indo-Pacific (Dechnik *et al.*, 2017). Modern species of *L.* gr. *kotschyanum* in the GBR have a wide depth distribution (0 to 20 m) and *H.* gr. *munitum* was recorded between 9 and 27 m (Dechnik *et al.*, 2017). Thus, the authors suggest that this algal assemblage was probably deposited in shallow to intermediate palaeo-water depths of 0 to 30 m.

Algal Assemblage 3 (A3) is dominated by laminar *Lithothamnion* spp. with associated thin crusts of *Lithophyllum* gr. *pustulatum*, *Peyssonnelia* and *Lithoporella* sp. (Fig. 5D) and characterises many crusts of the rhodolith facies. Modern Indo-Pacific CCA assemblages dominated by *Lithothamnion* and other Hapalidiales are characteristic of relatively deep waters below 20 – 30 m (Adey *et al.*, 1982; Lund *et al.*, 2000; Matsuda & Iryu, 2011; Bassi *et al.*, 2012).

Fossil assemblages dominated by *Lithothamnion* spp. commonly occur in deeper tropical settings (>20 m) or on shaded surfaces within reef frameworks (Webster *et al.*, 2009; Abbey *et al.*, 2011; Humblet *et al.*, 2019). Green calcareous *Halimeda* plates can also be associated with the coralline algal assemblage. Therefore, the authors suggest that this assemblage was deposited on a deeper reef slope in palaeo-water depths >20 m.

Larger benthic foraminifera assemblages (LBF)

The authors recognised 20 taxa of LBFs in thin sections. Community composition is more similar to nearby areas in Indonesia (Renema & Troelstra, 2001; Renema, 2003) than to the West Australia coast (Parker, 2009). The components that most stand out are the calcarinids, especially *Schlumbergerella floresiana* and *Calcarina* spp. (*C. hispida* gr., *C. spengleri, C. mayori*). *Schlumbergerella* have not been observed along the West Australia coast (Parker, 2009; Weinmann *et al.*, 2013) but *S. floresiana* occurs on nearby Ashmore Reef where it is most abundant foraminifer on the modern reef crest and back reef settings (Glenn & Collins, 2005). The foraminifers in the NWS cores can be grouped into two assemblages. Assemblage 1 (LBF1) is dominated by *S. floresiana* and *Amphistegina lobifera*, with associated *Amphisorus* spp., *C. hispida* gr. and *Peneroplis* spp. and is found in 12 thin sections (Fig. 5E and F). These taxa can occur *in situ* on the upper reef slope and reef flat, with a maximum depth of ~20 m, but with the highest densities at 0 to 10 m water depth, particularly on the reef crest when dominated by *S. floresiana.* Assemblage 2 (LBF2) is characterised by *Amphistegina radiata* and *Heterostegina depressa* (Fig. 5G). This assemblage was found in 16 thin sections and can be associated with *C. spengleri* and *Alveolinella quoyi* (Fig. 5H). On reefs in Indonesia the main taxa of this assemblage occur in deeper (coral) reef slope settings with coral rubble covered with crustose coralline algae at a depth range of 5 to 50 m (Renema & Troelstra, 2001).

Coralgal assemblages

Four main coralgal assemblages (Table 4, Fig. 6) were defined based on dominant coral, CCA and LBF compositions, as well as vermetid gastropod abundance. These assemblages represent various palaeo-environments, from very shallow, high-energy reef crests, upper and middle, intermediate-energy slopes, as well as sheltered back reef settings, based on comparisons with their modern counterparts, sedimentary facies associations and previously established fossil assemblages from the Indo-Pacific.

Coralgal assemblage 1 (C1) is the most common assemblage and is dominated by robust branching (corymbose/digitate) *Acropora* (i.e. *A. humilis, A. monticulosa, A. gemmifera*), branching *Stylophora pistillata* and *Porites* (*P. cylindrica, P. nigrescens*), associated *Isopora palifera* (sub-massive/encrusting) and *Montipora* (encrusting/branching) (Fig. 6A to C) with rare massive *Goniastrea, Goniopora* and *Cyphastrea* species. Fossil assemblages dominated by robust *Acropora/Isopora* species are commonly interpreted as growing in high-energy, shallow-water (<10 m) environments, typical of outer reef flats or upper reef slopes (Humblet *et al.*, 2019; Braga *et al.*, 2022). On the north-west Cape of Western Australia acroporids and encrusting *Montipora* commonly occur along shallow reef platforms in water depths of ~2.5 to 5 m, whereas *Porites* species dominate at slightly greater depths of ~4 to 6 m (Twiggs & Collins, 2010). Specifically, modern surveys at Ashmore Reef confirm that several *Acropora* species (i.e. *A. latistella, A. humilis, A. gemmifera*), *Isopora palifera* and *S. pistillata*, *P. cylindrica, P. nigrescens* which characterise this fossil assemblage, are all common in exposed, shallow-water settings <10 m (Kospartov *et al.*, 2006; Richards *et al.*, 2009; Ceccarelli *et al.*, 2011). This assemblage is also associated with shallow CCA (A1), LBF (LBF1) assemblages and abundant vermetid gastropods (mainly abundance category 3, 2) and therefore can be restricted to very shallow, high-energy reef crest-upper slope

settings <5 m deep (Dechnik *et al.*, 2017; Humblet *et al.*, 2019).

Coralgal assemblage 2 (C2) is dominated by corymbose branching *Acropora* spp. and merulinids (*Dipsastraea* gr. 2), with associated *Montipora* (encrusting-sub-massive) and *Seriatopora* (branching) (Fig. 6D). While common, the *Acropora* branches are heavily altered (dissolved/partially dissolved) limiting their taxonomic and morphologic identification. However, significantly, this coral community invariably occurs with relatively thin crusts of intermediate algae (A2) and few vermetid gastropods (category 1, 2), suggesting that this assemblage was deposited in intermediate reef slope settings, across a wide range of water depths (0 to 30 m) (Dechnik *et al.*, 2017; Humblet *et al.*, 2019).

Coralgal Assemblage 3 (C3) is characterised by corymbose/digitate *Acropora*, such as *A. digitifera* and more robust branching species (*A.* gr. 21 - *A. humilis, A. gemmifera, A. monticulosa*) and massive *Porites* (gr. 1 - *P. lutea, P. australiensis*), with associated merulinids (*Dipsastraea* gr. 1) (Fig. 6D). Similar to coralgal assemblage 1 (C1), this assemblage is associated with shallow CCA (A1), LBF (LBF1) assemblages and moderate abundance of vermetid gastropods (category 2) and is interpreted to be characteristic of shallow, high-energy reef settings <10 m (Dechnik *et al.*, 2017; Humblet *et al.*, 2019; Braga *et al.*, 2022).

Coralgal Assemblage 4 (C4) is rare, occurring only at the base of FPSO-E-C core. Columnar *Pavona clavus* (Fig. 6G) dominates this assemblage with associated branching *Acropora (*digitate*), Pocillopora*, encrusting *Montipora* and *Pavona explanulata*. Modern *P. clavus* typically occurs in semi-protected environments over a wide range of water depths (0 to mesophotic depths) (Veron & Pichon, 1979; CoralTraitDatabase, 2020; OBIS, 2020). Specifically, at Ashmore Reef *Pavona clavus* has been observed in lower reef slope and lagoonal environments (Kospartov *et al.*, 2006). The C4 corals are encrusted by thin crusts of intermediate CCA (A2) lacking vermetid gastropods and occur amongst a grainstone/packstone matrix containing the LBFs *Neorotalia calcar* and *Calcarina hispida*, which are characteristic of reef flat, back reef and lagoonal settings at Ashmore Reef (Glenn & Collins, 2005). However, they lack the exposed, reef crest *S. floresiana* most characteristic of LBF1. A broadly similar massive to columnar agariciid (*Gardinoseris planulata, Pavona maldivensis*) fossil assemblage (A3 in Gischler *et al.*, 2016) with similar CCA components occurs in the lower sections of Holocene reefs at Bora Bora where it indicates an intermediate-energy, fore reef environment, or sheltered reef flat or back reef setting (10 to 20 m). Thus, the authors interpret the C4 assemblage as having grown in an intermediate, backreef or lagoonal environment at >10 to 30 m palaeowater depth.

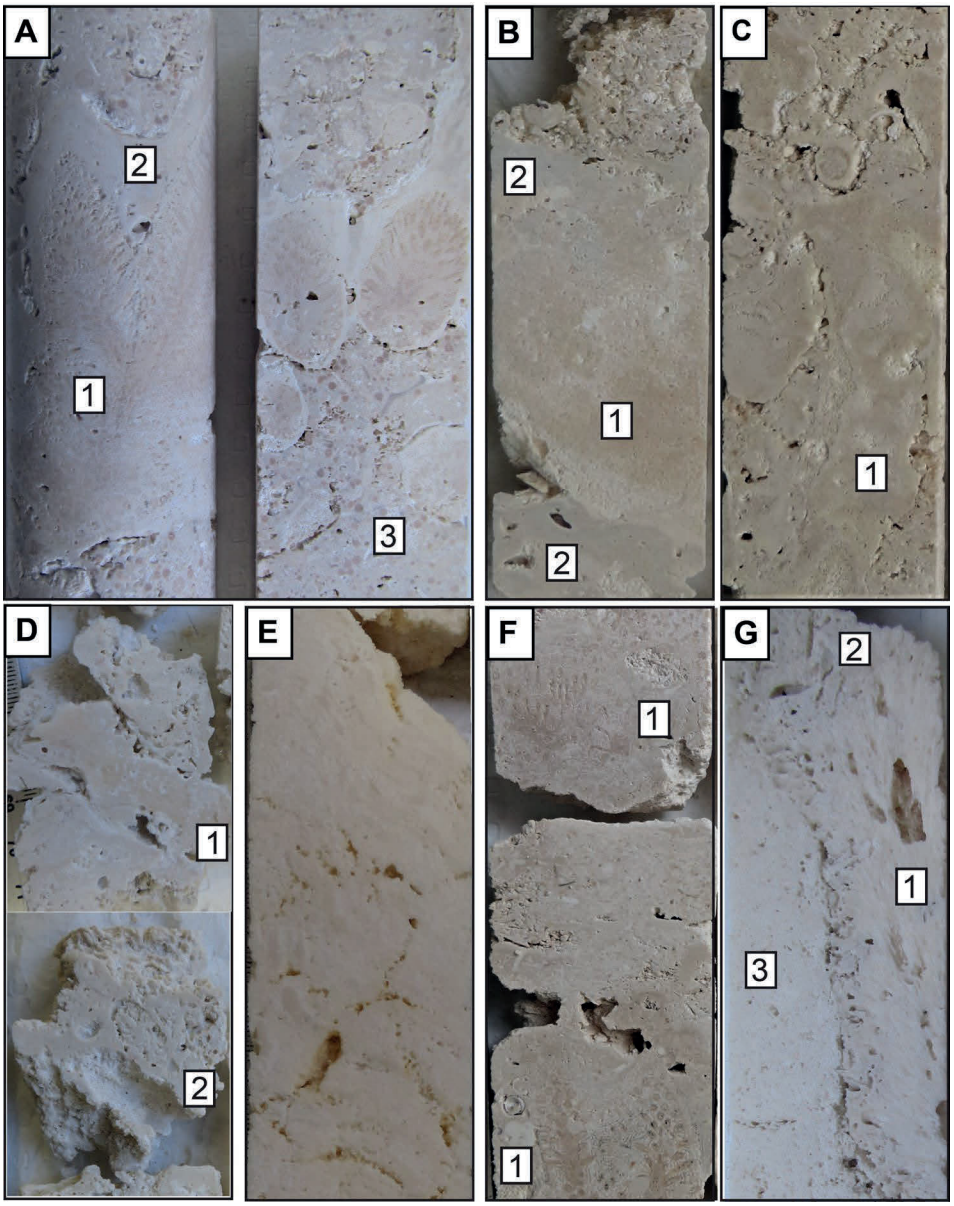

Fig. 6. Main coralgal assemblages observed in NWS cores. (A) Robust branching *Acropora monticulosa* (corymbose/digitate) (1), with branch tips encrusted by thick layers of *Porolithon* gr. *onkodes* (A1) and vermetid gastropods (2) (FPSO-E-C-1A-1) and associated grainstone/packstone sediments dominated by larger benthic foraminifera (*Schlumbergerella floresiana*) (LB1) that is characteristic of shallow, high-energy, upper reef crest-slope settings in <5 m water depths (C1 assemblage). (B) Submassive *Isopora palifera* (1) growing on and encrusted by thick crusts of coralline algae (2) (SWIFT-N-1C-4A) and (C) branching *Montipora* are also characteristic of the C1 assemblage (FPSO-NW-C-3A). (D) Partially (1) (FPSO-SW-S1-6A) to severely dissolved (2) (FPSO-SW-S1-7A) branching *Acropora* sp. covered with thin crusts of A2 coralline algae are characteristic of intermediate reef slope settings in 0 to 30 m water depths. (E) Massive *Porites* (SWIFT-MF-C-10B) and (F) robust branching *Acropora digitifera* (1) (SWIFT-N-1-C-6A) with associated thick crusts of A1 coralline algae that is characteristic of shallow, high-energy reef settings in <10 m water depths (C3 assemblage). (G) Columnar *Pavona clavus* (1) associated thins crusts of A2 coralline algae (2) and grainstone/packstone sediments (3) characteristic of deeper, backreef or lagoonal settings, >10 to 30 m (FPSO-E-C-10A (C4 assemblage). Core diameter is 4.5 cm in all images.

Mineralogical variations, diagenetic characteristics and environments

Visual observation of the cores, thin sections, SEM, XRD and hyperspectral data reveal a diverse suite of characteristics indicating both marine and meteoric diagenesis (Figs 7 to 10). The major downhole patterns are described below. The top few metres of the holes (~75 to 79 mbsl) are characterised by entirely marine diagenetic signatures. SEM and thin sections (Fig. 5B and C) reveal well-preserved coralline algae crusts and other bioclasts. Local minor pore filling cements consist of acicular aragonite, high-Mg calcite scalenohedral crusts and peloids (Fig. 8C), but no meteoric diagenetic overprint was observed. In contrast, both marine and meteoric diagenetic signatures are present from ~80 to 90 mbsl. In some sections aragonite coral microstructure is pristine (Fig. 8A and B), whilst in others a heterogeneous meteoric overprint is characterised by partial dissolution of coral skeletons and replacement with low-Mg calcite cements. Pore-filling cements are predominantly isopachous dogtooth low-Mg calcite, suggesting a meteoric phreatic environment (Fig. 8D to F).

This meteoric overprint and associated mineralogic changes are complex and spatially variable at the core scale with the hyperspectral image and numerical data sets showing many sections where corals are altered to calcite, while others retain their aragonitic skeleton (i.e. $CaCO_3$ classification, feature characteristics, calcite purity; Figs 9 and 10). In these cases, SEM and thin section data clearly show that significant elements of pristine aragonite coral skeletons remain (Fig. 8A and B) consistent with XRD measurements up to 97.5% aragonite from representative corals (Table 6).

However, below ~90 mbsl the meteoric diagenetic signatures become more pervasive and complex. Mouldic porosity is evident in hand specimens from ~90 to 95 mbsl with many dissolved and partially dissolved corals (Figs 6D and 7C). SEM and thin sections show these heterogeneously dissolved and recrystallised corals have been mostly replaced by low-Mg calcite but locally some skeletal aragonite remains (Fig. 8G to J). Low Mg calcite also occurs occluding coral pore spaces and euhedral rhombohedral crystals that are morphologically consistent with dolomite also occur (Fig. 8H and I). These same rhombohedral crystals also partially replace microbial carbonates in some coral pores (Fig. 8J). The presence of dolomite in corals from these depths is supported by hyperspectral data (e.g. Fig. 9B – $CaCO_3$ classification as green pixels in SWIFT-N1-C-6-7) and was confirmed by XRD measurements reporting 11% dolomite.

Two notable palaeosol horizons occur between 79 to 82 mbsl (Fig. 7A and B) and 89 to 92 mbsl (Fig. 7F) marking changes in the down-hole lithologic, mineralogic and diagenetic features described above. These palaeosols consist of reddish-brown grainstone-packstone as much as several cm-thick and multi-layered in some cores. Hyperspectral imaging (Fig. 7I) confirms the abundance of clay (kaolinite) within these layers. Thin section analysis reveals extensive dissolution within these sections and pisoids clearly penetrate into the surrounding carbonate substrate (CCA and LBF packstones), indicating that they post-date these sediments. Hyperspectral proxy imagery and numerical data also record major changes in carbonate mineralogy at or near these two main palaeosol horizons (Figs 9 and 10). This is best observed in FPSO-NW-C-1, SWIFT-N-1-C and SKUA-10/11, which have the highest density of hyperspectral proxy measurements that together suggests that these palaeosol horizons represent major chrono-stratigraphic boundaries (Fig. 10).

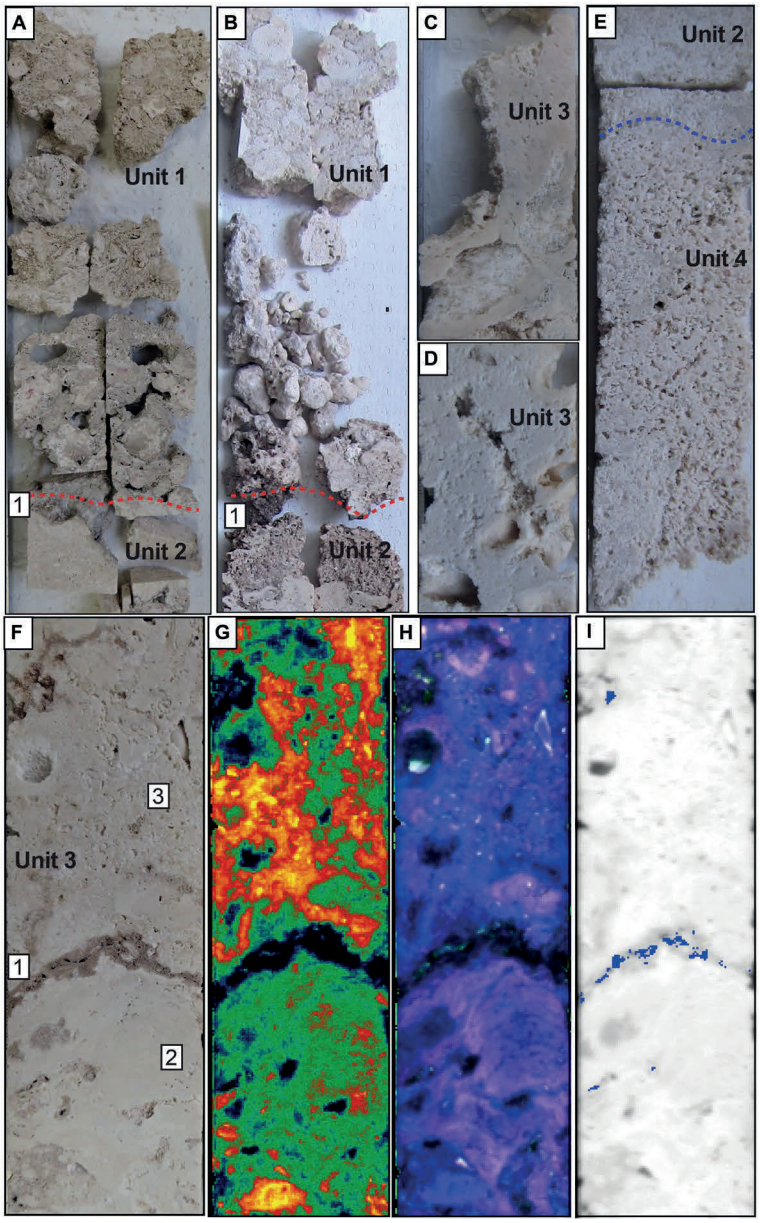

Fig. 7. Representative images showing characteristics of the major chrono-stratigraphic units, their boundaries and macro-scale diagenetic features. (A) and (B) Core images showing the Unit 1 (Rhodolith floatstone-dominated facies) and 2 (Coral framestone-dominated facies) boundary characterised by a distinct palaeosol horizon (1) (SWIFT-N-1-C-1A; FPSO-SW-C1-1A). (C) and (D) Core images of Unit 3 (Coral framestone-dominated facies) characterised by dissolved and partially dissolved (mouldic porosity) robust *Acropora* branches with grainstones/packstones (FPSO-E-C-8A). (E) Core image showing the boundary (dashed line) between Unit 2 and 4 that is marked by a sharp contact and clean grainstones facies that lack corals (FPSO-SW-C1-6A). (F) Core image showing the characteristics of the 2nd major palaeosol marking the Unit 2 and 3 boundary (FPSO-NW-C-7A-2). These multiple red, brown soils layers (1) penetrate into Unit 3, characterised here by thick coralline algal bindstone (2) and (3) packstone facies. The main lithology types, and macro-scale diagenetic features, are accurately discriminated by the high-resolution hyperspectral imagery: (G) calcite purity index, (H) intensity of absorption features of water, OH and carbonate displayed as red, green and blue; (I) clay (kaolinite) mapped from its diagnostic absorption feature at 2207 nm (blue pixels) is clearly visible in the palaeosol. Core diameter is 4.5 cm in all images.

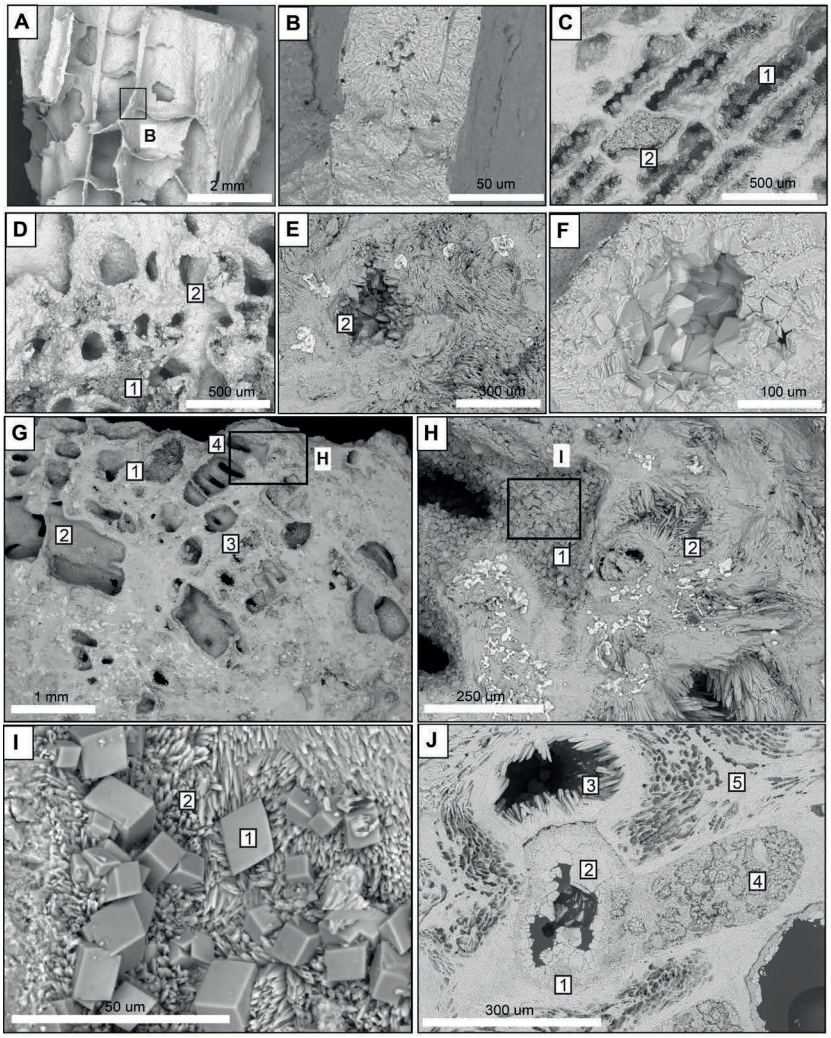

Fig. 8. Representative SEM images showing characteristic, micro-scale features indicative of both marine and meteoric diagenetic environments. (A) Well preserved *Platygyra sinensis* with large open pore spaces, free of internal cements and (B) close up of well-preserved fibrous, coral skeletal microstructure with minor microboring (FPSO-NW-C-1A). (C) *Goniopora* showing key features of marine diagenesis including acicular aragonite fringing cements (1) and peloidal high-Mg calcite (2) within interseptal spaces (SWIFT-N-1-C-1A-3). (D) *Montipora* showing partial dissolution of coral skeleton (1) and blocky, low-Mg calcite meteoric cement (SKUA-10-11-C1-3A1). (E) *Acropora* with pore lined with low-Mg calcite cement (2) as a result of meteoric diagenesis (FPSO-SW-S1-3B). (F) Blocky, low-Mg calcite meteoric cement in *Acropora* (WHP-EP-S-3A-1). (G) *Acropora* skeleton showing various marine and meteoric cements including an aragonite fringe (1), high-Mg calcite peloids (2), low-Mg calcite (3); and dolomite (4) in the region of higher magnification shown as box H (SWIFT-N-1-C-6A). (H) Enlargement showing dolomite cement on aragonite (1) and large secondary acicular aragonite cements (2). Region of higher magnification shown as box I. The bright white material is secondary halite. (I) Enlargement of rhombohedral dolomite cement (1) overlying fine acicular, possibly syntactic aragonite cement (2). (J) Polished SEM image of SWIFT-N-1-C-6A showing complex relationships between different phases of marine and meteoric diagenetic products. Blocky dolomite cement partially replacing or nucleated on high-Mg calcite lining pore in coral skeleton (1), directly overlain by blocky low-Mg calcite cement not quite occluding the pore (2). Secondary acicular aragonite cement lines second pore (3). High-Mg calcite microbialite containing trapped and bound sediment is partially replaced by dolomite in pore (4) and remaining elements of original coral aragonite skeleton (5) have undergone partial dissolution resulting in scalloped pattern.

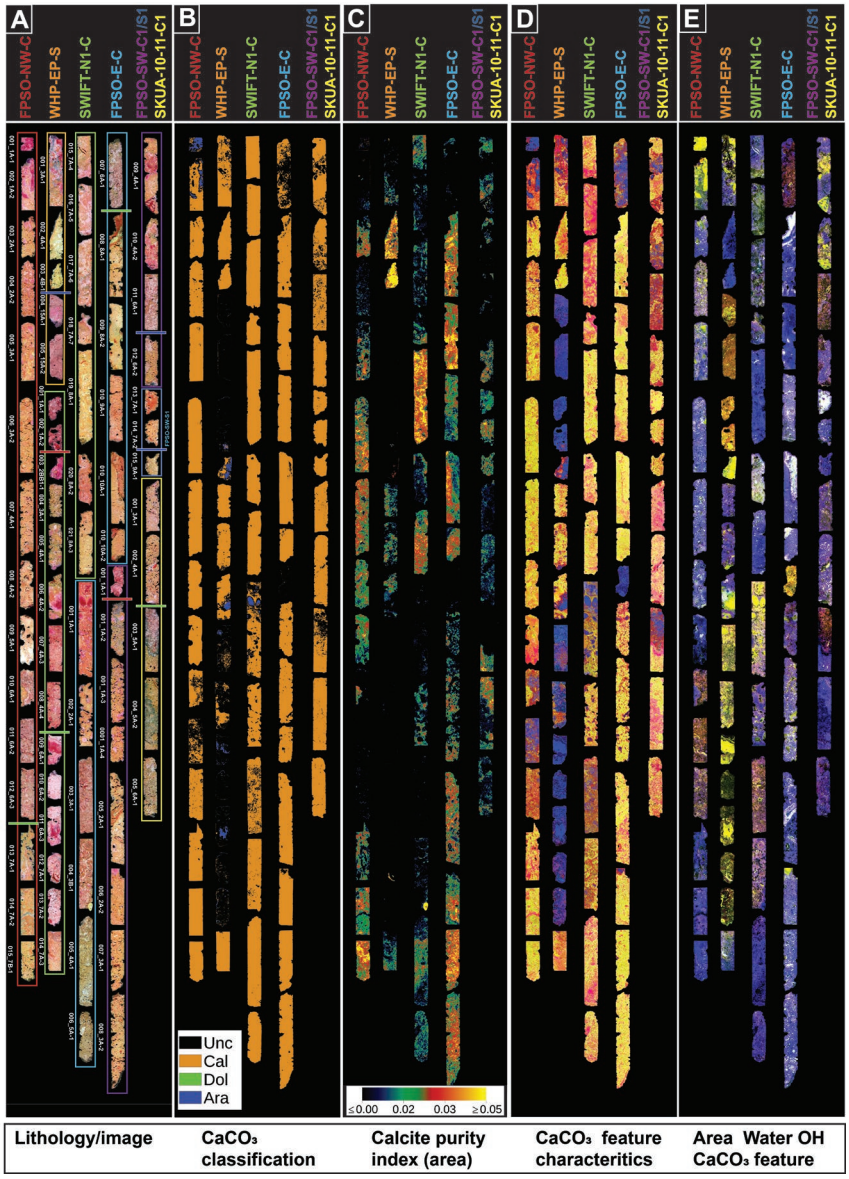

Fig. 9. Representative images showing the major hyperspectral characteristic of NWS shelf cores. (A) False colour composite image showing the main lithologic characteristics of the main sites and representative core section. (B) Classified image of the carbonates (calcite, aragonite, dolomite, unclassified) derived using the method of Murphy *et al.*, (2017). (C) Image showing calcite purity index based on the area of the minor (secondary) carbonate absorption feature at 1880 nm, showing more aragonitic calcite phases (black), poorly crystalline calcite (blue tones) and progressively more crystalline calcite phases (red through yellow tones). (D) Image showing $CaCO_3$ feature characteristics based on the wavelength position, intensity and asymmetry of the primary carbonate absorption feature located at ~2331 nm, displayed as red, green and blue, respectively. The image highlights the primary carbonate phases in the image with red tones indicating less crystalline calcite, green tones indicating crystalline calcite and blue tones indicating aragonite. Intermediate colours represent mixtures of these three phases. (E) Image showing the area of the absorption features of water, OH and carbonate displayed as red, green and blue, respectively. Yellow tones show aragonitic phases, containing large amounts of water and OH. Blue tones highlight more crystalline calcite phases with little or no water absorption, white and reddish tones show carbonate phases with high (white) and low (red tones) water, OH and carbonate absorption, probably transitional between aragonite and calcite.

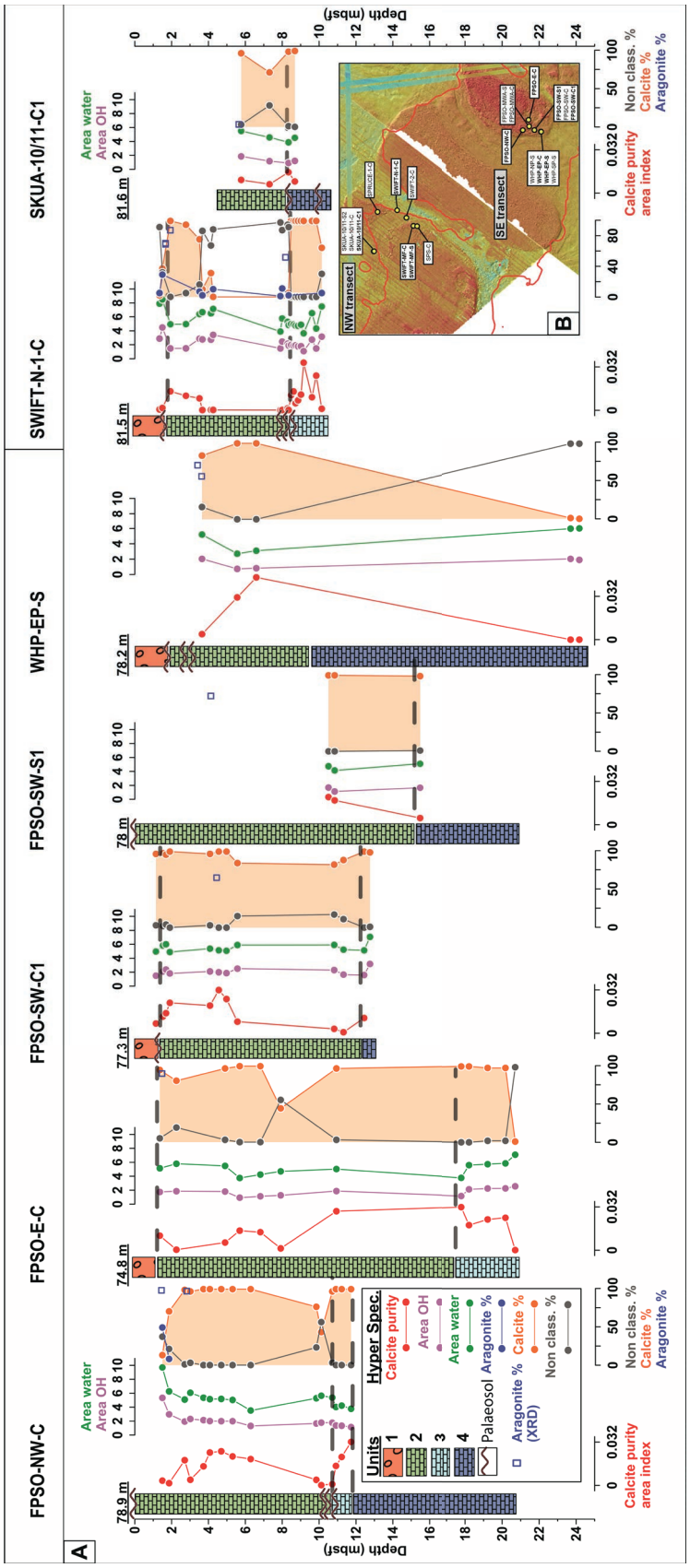

Fig. 10. Hyperspectral proxy data versus depth in representative NWS cores. (A) Simplified logs showing down hole variation in numerical hyperspectral proxy data (calcite purity area index, area of the absorption features of water and OH, carbonate classification based on percent pixels) and XRD (% aragonite – blue squares). The grey dashed lines represent boundaries of the four chronostratigraphic units (Units 1–4) that also correspond to major changes in the hyperspectral proxy data and in some cases are marked by palaeosol horizons. To illustrate the down hole patterns in carbonate classification, the % of pixels classified as calcite are shaded with a light orange fill. (B) Core locations and their geomorphic context on the platforms.

Radiometric dating *vs*. depth

Radiocarbon measurements were made on 24 carbonate samples (corals, coralline algae and molluscs) from core depths of 75.62 to 90.64 mbsl (Fig. 11, Table 5). Calibrated ages range from 10.7 to 44.8 ka, spanning MIS 3 to MIS 1 during the late deglacial. Two samples at the base of SWIFT-MF-C and FPSO-NW-C could not be calibrated because they contain no modern carbon (i.e. they are too old and radiocarbon 'dead'). Four ages from well preserved coralline algae (Fig. 7) from the top 1 m of SWIFT-N-1-C, WHP-EP-C, FPSO-SW-C1 and FPSO-E-C range from 10.4 to 13.1 ka confirming that these rhodoliths are late deglacial in age. Samples below ~81 to 83 mbsl in the coral-dominated sections of the holes down to ~89 mbsl cluster towards the end of MIS 3 and into MIS 2. However, based on SEM, hyperspectral, petrologic and XRD data, some of these samples have undergone varying degrees of meteoric diagenetic alteration, suggesting subaerial exposure. This is clearly illustrated in Fig. 11, showing age versus depth of the coral samples plotted with their corresponding percent aragonite and their relationship to RSL in the region. For example, several coral samples (e.g. SKUA-10-11-C1-3A – 21.3 ka; SWIFT-MF-C-4A – 27.9 ka) plot well above the position of RSL during MIS 2 in the region (Ishiwa *et al.*, 2019a), consistent with their almost entire recrystallisation to calcite based on mineralogical data. Eleven corals in this middle section of the holes range in age between ~27.9 to 39.7 ka with aragonite values between 51.6 and 97.5%. However, the SEM observations, hyperspectral and XRD data also show that this diagenesis is highly variable; and that the authors consider coral samples FPSO-NW-C-1A-1 (97.5%), FPSO-NW-C-2A (96.4%), and less so FPSO-E-C-1A-2 (89.4%) and SWIFT-N-1-C-2BB1 (86.9%), to yield the most reliable ^{14}C-ages of 35.0 to 39.7 ka in these cores. This is consistent with the paired U/Th ages on the same coral samples (FPSO-NW-C-1A-1, FPSO-NW-C-2A, FPSO-E-C-1A-2) that returned three ages between 39.23 and 45.95 ka in MIS 3. These corals were evaluated for ^{232}Th, initial ^{234}U/^{238}U activity ratios (reported as $d^{234}U_i$ in permil) and also for anomalous ^{238}U concentrations, which can indicate detrital Th contamination or open-system diagenesis (Dechnik *et al.*, 2017). These samples passed those criteria and have initial $d^{234}U_i$(‰) values between 141.64 and 142.49 $\pm$ 0.9 to 1.1‰, well within recently published screening tolerances (140 $\pm$ 8‰) (see Chutcharavan *et al.*, 2018 for recent review) for MIS 3 corals (Table 6). Furthermore, samples FPSO-NW-C-1A-1 (39.23 ka) and FPSO-NW-C-2A (44.74 ka) from the same hole, are *in-situ* and in stratigraphic order. The authors also note that the U/Th ages are 2.56 to 7.9 kyr older than their corresponding radiocarbon ages, an offset consistent with other MIS 3 corals from the adjacent uplifted reefs of the Huon Peninsula (Yokoyama *et al.*, 2000). Two coralline algal samples (WHP-EP-S-3A-2, FPSO-NW-C-6A-2) and one mollusc sample (SKUA-10-11-C1-3A2) from this same middle section of the cores gave ^{14}C-ages between 31.5 to 40.2 ka. However, only WHP-EP-S-3A-2 (33.15 ka) is considered moderately reliable based on SEM observations and its consistent stratigraphic position.

Finally, the three samples below ~89 m (SWIFT-N-1-C-6A, SWIFT-MF-C-10B, FPSO-NW-C-7B) are radiocarbon 'dead' and/or XRD and SEM observations confirm they have suffered the most severe diagenetic alteration, including dolomitization (XRD 11.1%) (Figs 7 to 9). Taken together, this indicates the presence of a stratigraphically deeper, coral-dominated section that is both diagenetically distinct and older than 50 ka.

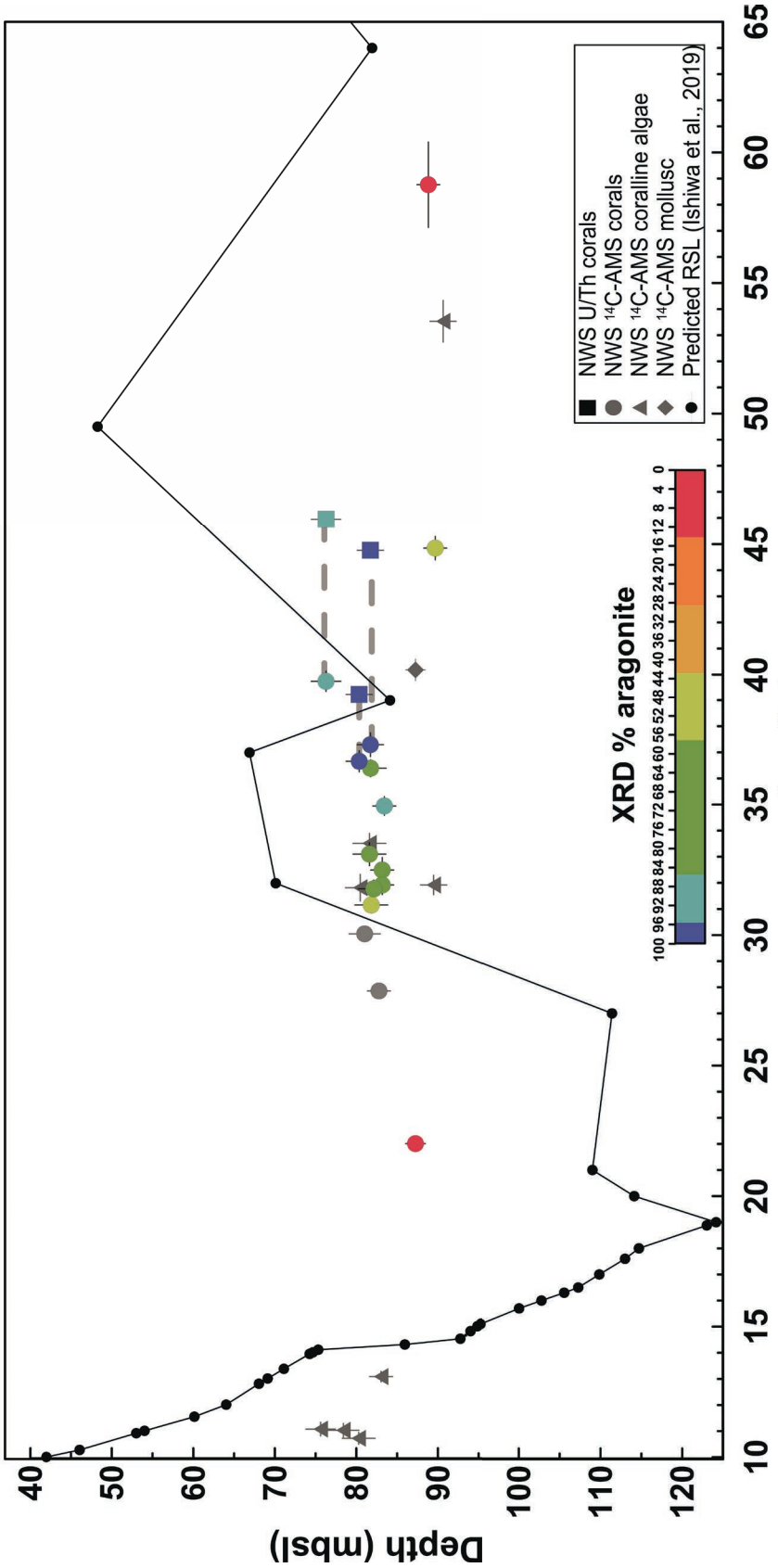

Fig. 11. Summary of age *vs.* depth data from the NWS cores. Sample depths are plotted as metres below sea-level (mbsl) and include the tidal error but are not corrected for regional subsidence. The predicted RSL (black points and line) for the NWS based on GIA modelling is shown for reference (Ishiwa *et al.*, 2019a). In some cases, the size of the symbol is larger than the age error. Coral samples are colour coded with their respective % aragonite as measured by quantitative XRD. The grey dashed lines represent the age offset between closed-system U/Th ages and calibrated ^{14}C-AMS ages on the same coral sample (see Tables 5 and 6 for details). The grey coloured symbols represent samples that lack XRD data.

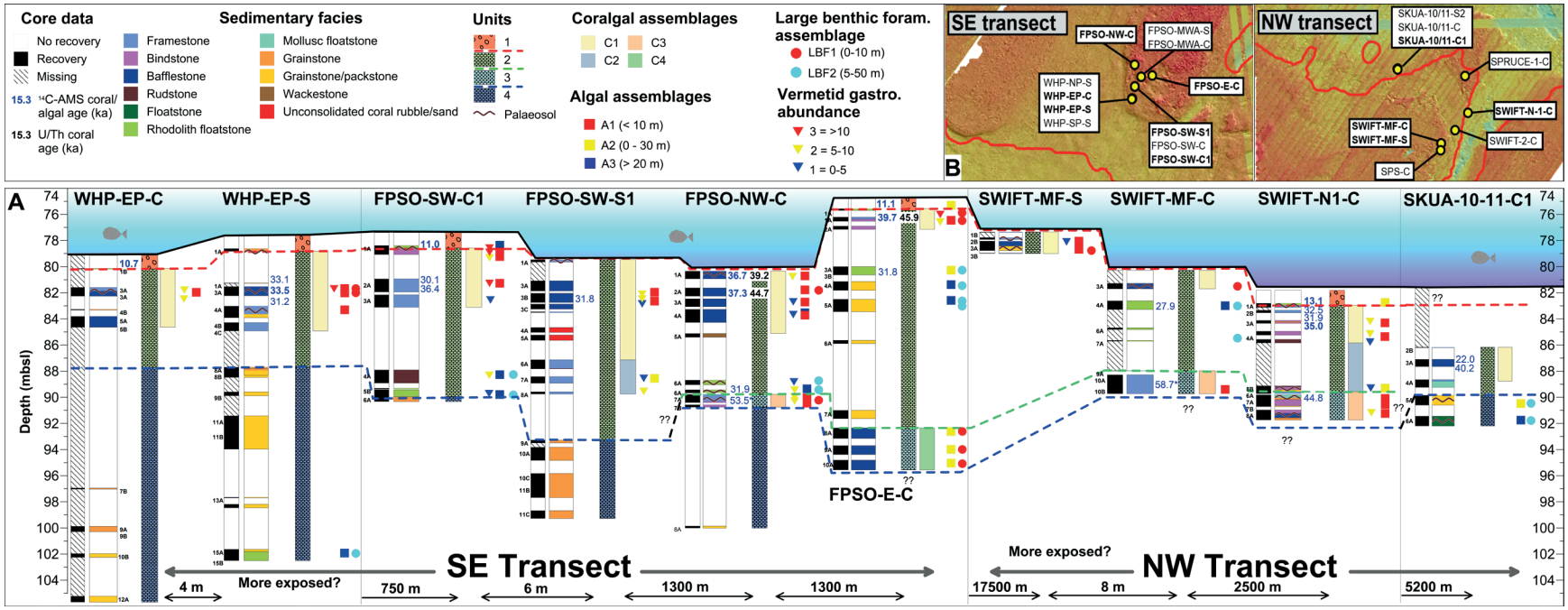

Fig. 12. Summary of sedimentary facies, chrono-stratigraphic units, reef biota and radiometric data for the SE and NW drill transects on the NWS. (B) Simplified stratigraphic sections showing the distribution of recovered core intervals, coral, algal, large benthic foraminifera assemblages, vermetid gastropod abundance, palaeosols horizons and U–Th and ^{14}C-AMS ages (bold values represent reliable ages). The boundaries of the four chrono-stratigraphic units (Units 1 to 4) are represented by the dashed coloured lines. The x-axis represents the distance between the cores and is schematic; (A) gives the actual core locations and their geomorphic context on the platforms.

Table 5 (first section). Radiometric data from the carbonate deposits recovered from the NWS cores.

Sample ID	Lab code	Tran-sect	Depth below sea-level (mbsl)	Tidal depth ±(m)	Dated Lithology	Genera/ lithology
SKUA-10-11-C1-3A1	YAUT-028036	NW	87.25	1.2	Coral	*Montipora*
SKUA-10-11-C1-3A2	YAUT-028037	NW	87.25	1.2	Mollusc	
SWIFT-N-1-C-1A-2	YAUT-028032	NW	83.03	1.4	Coralline algae	Rhodolith
SWIFT-N-1-C-1A-1	YAUT-028031	NW	83.17	1.4	Coral	*Goniopora*
SWIFT-N-1-C-1A-3	YAUT-028033	NW	83.17	1.4	Coral	*Goniopora*
SWIFT-N-1-C-2BB1	YAUT-037437	NW	83.43	1.4	Coral	*Favites* gr. 1
SWIFT-N-1-C-6A	YAUT-037832	NW	89.68	1.4	Coral	*Acropora*
SWIFT-MF-C-4A	YAUT-037438	NW	82.77	1.4	Coral	*Acropora*
SWIFT-MF-C-10B	YAUT-037439	NW	88.83	1.4	Coral	*Acropora*
WHP-EP-C-1BB1	YAUT-028029	SW	80.29	2	Coralline algae	Rhodolith
WHP-EP-S-3A-1	YAUT-028026	SW	81.61	2	Coral	*Acropora*
WHP-EP-S-3A-2	YAUT-028028	SW	81.61	2	Coralline algae	Fragments
WHP-EP-S-3A	YAUT-037829	SW	81.83	2	Coral	*Acropora*
FPSO-SW-C1-1A	YAUT-028023	SW	78.41	1.9	Coralline algae	Rhodolith
FPSO-SW-C1-2A	YAUT-028024	SW	81.02	1.9	Coral	*Acropora*
FPSO-SW-C1-2A	YAUT-037826	SW	81.74	1.9	Coral	*Acropora*
FPSO-SW-S1-3B	YAUT-037828	SW	82.13	1.9	Coral	*Acropora*
FPSO-NW-C-1A-1	YAUT-028025	SW	80.35	1.6	Coral	*Platygyra sinensis*
FPSO-NW-C-2A	YAUT-037836	SW	81.72	1.6	Coral	*Porites*
FPSO-NW-C-6A-2	YAUT-037831	SW	89.48	1.6	Coralline algae	Rhodolith
FPSO-NW-C-7B	YAUT-037833	SW	90.64	1.6	Coralline algae	Rhodolith
FPSO-E-C-1A-1	YAUT-028018	SW	75.62	1.8	Coralline algae	Rhodolith
FPSO-E-C-1A-2	YAUT-028019	SW	76.28	1.8	Coral	*Acropora*
FPSO-E-C-3B	YAUT-037837	SW	80.48	1.8	Coralline algae	Rhodolith

Table 5 (second section). Radiometric data from the carbonate deposits recovered from the NWS cores.

Sample ID	Assem.	XRD[a]	Aragonite	Calcite	Hi-Mg Calcite	Dolomite	SEM	Context info.[b]
SKUA-10-11-C1-3A1	C1	3.3	3.3	93.1	3.6		Y	IS
SKUA-10-11-C1-3A2	C1							NEI
SWIFT-N-1-C-1A-2	A2							IS
SWIFT-N-1-C-1A-1	C1	69.9	69.9	14.2	17.8		Y	IS
SWIFT-N-1-C-1A-3	C1	68.6	68.6	16.1	15.2		Y	IS
SWIFT-N-1-C-2BB1	C1	86.9	86.9	10	3.1		Y	IS
SWIFT-N-1-C-6A	C2	51.6	51.6	17.6	19.7	11.1	Y	IS
SWIFT-MF-C-4A	C1							NEI
SWIFT-MF-C-10B	C3	4.2	4.2	95.8			Y	IS
WHP-EP-C-1BB1	-						Y	IS
WHP-EP-S-3A-1	C1	70.5	70.5	18	11.5			IS
WHP-EP-S-3A-2	C1						Y	IS
WHP-EP-S-3A	C1	56	56	20.5	23			IS

FPSO-SW-C1-1A	A3						Y	IS
FPSO-SW-C1-2A	C1						Y	IS
FPSO-SW-C1-2A	C1	65	65	35			Y	IS
FPSO-SW-S1-3B	C1	72.1	72.1	20.1	7.8			IS
FPSO-NW-C-1A-1	C1	97.5	97.5	1.9	0.7		Y	IS
FPSO-NW-C-2A	C1	96.4	96.4	3.6			Y	IS
FPSO-NW-C-6A-2	A3							IS
FPSO-NW-C-7B	C3						Y	IS
FPSO-E-C-1A-1	-						Y	IS
FPSO-E-C-1A-2	C1	89.4	89.4	5	5.6			IS
FPSO-E-C-3B	-						Y	IS

Table 5 (third section). Radiometric data from the carbonate deposits recovered from the NWS cores.

Sample ID	**Palaeo-water depth max (m)**	**Palaeo-water depth min (m)**	**d^{13}C (‰)**	**±1s**	**^{14}C age (yr BP)**	**±1s**	**Calibrated age (ka)[c]**	**Lower cal. range BP**
SKUA-10-11-C1-3A1	10	0	2.73	1.36	18961	58	22.0	21.707
SKUA-10-11-C1-3A2	10	0	5.74	0.79	36127	175	40.2	39.749
SWIFT-N-1-C-1A-2	30	0	21.1	4.24	11817	51	13.1	12.875
SWIFT-N-1-C-1A-1	5	0	2.19	2.88	29144	110	32.5	32.028
SWIFT-N-1-C-1A-3	5	0	-0.67	3.44	28775	109	31.9	31.564
SWIFT-N-1-C-2BB1	5	0	-3.7	2.5	31429	130	35.0	34.596
SWIFT-N-1-C-6A	30	0	3.6	2.3	43132	293	44.8	44.375
SWIFT-MF-C-4A	10	0	0.3	2.8	24660	86	27.9	27.631
SWIFT-MF-C-10B	10	0	0.9	3.3	58765	1636	58.8	
WHP-EP-C-1BB1	30	0	14.2	3.94	9952	47	10.7	10.486
WHP-EP-S-3A-1	5	0	-4.28	8.52	29548	131	33.1	32.672
WHP-EP-S-3A-2	5	0	3.63	1.98	29900	115	33.5	33.15
WHP-EP-S-3A	5	0	-2.3	5.6	28017	109	31.2	30.95
FPSO-SW-C1-1A	-	>20	19	4.61	10165	51	11.0	10.761
FPSO-SW-C1-2A	5	0	1.49	8.76	26772	116	30.1	29.803
FPSO-SW-C1-2A	5	0	-3.6	3.2	32844	136	36.4	36.08
FPSO-SW-S1-3B	5	0	-6.4	4.1	28653	107	31.8	31.45
FPSO-NW-C-1A-1	5	0	4.19	3.11	33094	144	36.7	36.268
FPSO-NW-C-2A	5	0	10.4	3.1	33602	141	37.3	36.847
FPSO-NW-C-6A-2	-	>20	3.6	4.3	28774	107	31.9	31.563
FPSO-NW-C-7B	10	0	5.3	1.9	53535	796	53.5	
FPSO-E-C-1A-1	30	0	-9.86	2.74	10192	42	11.1	10.804
FPSO-E-C-1A-2	5	0	8.34	3.31	35659	172	39.7	39.344
FPSO-E-C-3B	30	0	8.7	7.4	28687	122	31.8	31.435

Table 5 (fourth section). Radiometric data from the carbonate deposits recovered from the NWS cores.

Sample ID	Upper cal range BP	2s age range (ka)	Lower	Upper	Mean 2s error (kyr)	U-Th age (ka)[d]	±2s (kyr)	U/Th Corrected depth below sea-level (mbsl)[e]	Corrected depth below sea level (mbsl)[e]	Chrono-strat unit
SKUA-10-11-C1-3A1	22.237	21.707-22.237	0.272	0.258	0.26				82.9	2
SKUA-10-11-C1-3A2	40.564	39.749-40.564	0.414	0.401	0.41				79.2	2
SWIFT-N-1-C-1A-2	13.264	12.875-13.264	0.199	0.19	0.19				80.4	1
SWIFT-N-1-C-1A-1	32.971	32.028-32.971	0.478	0.465	0.47				76.7	2
SWIFT-N-1-C-1A-3	32.475	31.564-32.475	0.371	0.54	0.46				76.8	2
SWIFT-N-1-C-2BB1	35.287	34.596-35.287	0.361	0.33	0.35				76.4	2
SWIFT-N-1-C-6A	45.349	44.375-45.349	0.45	0.524	0.49				80.7	3
SWIFT-MF-C-4A	28.211	27.631-28.211	0.247	0.333	0.29				77.2	2
SWIFT-MF-C-10B		-	1.636	1.636	1.64				77.1	3
WHP-EP-C-1BB1	11.014	10.486-11.014	0.229	0.299	0.26				78.1	1
WHP-EP-S-3A-1	33.586	32.672-33.586	0.442	0.472	0.46				75.0	2
WHP-EP-S-3A-2	33.891	33.15-33.891	0.377	0.364	0.37				74.9	2
WHP-EP-S-3A	31.463	30.95-31.463	0.217	0.296	0.26				75.6	2
FPSO-SW-C1-1A	11.215	10.761-11.215	0.261	0.193	0.23				76.2	1
FPSO-SW-C1-2A	30.356	29.803-30.356	0.26	0.293	0.28				75.0	2
FPSO-SW-C1-2A	36.783	36.08-36.783	0.321	0.382	0.35				74.5	2
FPSO-SW-S1-3B	32.142	31.45-32.142	0.336	0.356	0.35				75.8	2
FPSO-NW-C-1A-1	37.059	36.268-37.059	0.401	0.39	0.40	39.23	0.19	72.5	73.0	2
FPSO-NW-C-2A	37.814	36.847-37.814	0.455	0.512	0.48	44.74	0.20	72.8	74.3	2
FPSO-NW-C-6A-2	32.463	31.563-32.463	0.37	0.53	0.45				83.1	2
FPSO-NW-C-7B		-	0.796	0.796	0.80				79.9	3
FPSO-E-C-1A-1	11.234	10.804-11.234	0.262	0.168	0.22				73.4	1
FPSO-E-C-1A-2	40.149	39.344-40.149	0.384	0.421	0.40	45.95	0.22	67.1	68.3	2

FPSO-E-C-3B	32.268	31.435-32.268	0.508	0.533	0.52		74.1	2

[a]XRD value represents the % aragonite content of the measured corals.
[b]Special attention was given to establishing the context of each coral within each cored section. A combination of criteria was used to distinguish in situ corals from allochthonous rubble and/or drilling disturbance. Corals were classified as either *In-Situ* (IS), Not Enough Information (NEI) or Not *In-Situ* (NIS) based on criteria established in Humblet & Webster (2017).
[c]Only the samples in bold gave reliable ages and are plotted on Fig. 13 with the other relevant relative sea level indicators and paleo-oceanographic proxy data from the region.
[d]See Table 6 for the full details of the U/Th data.
[e]The sample depths are corrected to account for the long term subsidence rate (0.2 mm/yr) reported for the region since the Last Interglacial (Collins *et al*., 2011; Solihuddin *et al*., 2016).

Table 6. U-series coral measurements and ages recovered from the NWS cores.

Sample Name	U (ppm)	±2s	^{232}Th (ppb)	2σ	(^{230}Th/ ^{232}Th)	2σ	(^{230}Th / ^{238}U)	2σ	(^{234}U/ ^{238}U)	2σ	Corr. initial (^{234}U/ ^{238}U)[a]	2σ
FPSO-E-C-1A-2	3.5890	0.0019	1.925	0.008	2212	11	0.3910	0.0013	1.1270	0.0007	1.1446	0.0008
FPSO-E-C-1A-2	3.5861	0.0020	1.919	0.007	2213	12	0.3903	0.0017	1.1285	0.0008	1.1462	0.0009
FPSO-NW-C-1A-1	2.4214	0.0013	1.675	0.003	1500	7	0.3420	0.0015	1.1262	0.0009	1.1410	0.0010
FPSO-NW-C-1A-1	2.4196	0.0011	1.684	0.005	1497	7	0.3433	0.0012	1.1273	0.0010	1.1423	0.0011
FPSO-NW-C-2A	3.0382	0.0015	1.714	0.005	2047	11	0.3806	0.0017	1.1245	0.0010	1.1413	0.0011
FPSO-NW-C-2A	3.0384	0.0013	1.709	0.005	2063	9	0.3825	0.0011	1.1266	0.0007	1.1437	0.0008

Table 6 continuation. U-series coral measurements and ages recovered from the NWS cores.

Sample Name	$d^{234}U_i$ (‰)[b]	2σ	Uncorr. ^{230}Th age (ka)[c]	2σ	Corr. ^{230}Th age (ka)	2σ	Age (ka)[d]	2σ	$d^{234}U_i$ (‰)[b]	2σ
FPSO-E-C-1A-2	144.6	0.8	46.06	0.20	46.04	0.20				
FPSO-E-C-1A-2	146.2	0.9	45.87	0.24	45.86	0.24	45.95	0.22	145.41	0.89
FPSO-NW-C-1A-1	141.0	1.0	39.18	0.21	39.16	0.21				
FPSO-NW-C-1A-1	142.3	1.1	39.31	0.16	39.29	0.16	39.23	0.19	141.64	1.07
FPSO-NW-C-2A	141.3	1.1	44.67	0.24	44.66	0.24				
FPSO-NW-C-2A	143.7	0.8	44.84	0.16	44.83	0.16	44.74	0.20	142.49	0.94

[a]Nu Plasma MC-ICP-MS ^{230}Th ages and geochemical data with 2σ errors. Activity ratios calculated using decay constants of Cheng *et al*. (2000). Values have been corrected for laboratory procedural blanks.

[b]$d^{234}U_i$ = [(234U/238U)-1] x 1000. All values meeting screen tolerances for corals 17 to 60 ka (Chutcharavan *et al.*, 2018)

[c]Uncorrected ^{230}Th age calculated using Isoplot 3.75 program (Ludwig, 2012).

[d]Interpreted ages calculated by using mean for the individual sub samples of each coral. Interpreted closed-system ages are highlighted in bold.

NWS chrono-stratigraphic units, biotic distributions and successions

Four chrono-stratigraphic units were defined based on distinct lithologic, reef assemblage, mineralogic and chronologic variations (Fig. 12). Unit 1 is the top-most unit observed at most sites (WHP-EP-C, WHP-EP-S, FPSO-SW-C1, FPSO-E-C, SWIFT-N1-C) forming a 1m-thick deposit at the sea floor that is bounded at its base by a major palaeosol. Comprised of rhodolith floatstone facies, this unit was deposited in intermediate (0 to 30 m) to deeper (>20 m) reef slope settings between 13 and 10 ka. Mineralogical and SEM data confirm that Unit 1 was exposed only to marine diagenesis. Unit 2 was observed across all sites, in rare cases (FPSO-NW-C) directly at the sea floor, and is marked at its top by the first major palaeosol ~79 to 80 mbsl (base of Unit 1). This unit is ~10 to 15 m-thick and characterised by a clear shallowing-upward succession. *In situ*, coralgal-dominated bindstones, framestones and bafflestones are common between ~80 to 90 mbsl and, below this, deeper reef slope, grainstone/packstone, floatstone and rudstone facies occur. Mineralogical and SEM data confirm that Unit 2 was exposed to both marine and meteoric diagenesis but reliable U/Th and ^{14}C-AMS ages from pristine corals span 36.7 to 45.8 ka at the top of this unit. A major change in lithology, assemblage and mineralogic characteristics marks the base of this unit. At sites FPSO-NW-C, FPSO-E-C, SWIFT-C and SWIFT-NI-C the second major palaeosol horizon, consisting of multiple closely spaced but distinct soil layers at the base of the unit ~90 mbsl marks the start of a second coralgal-dominated reef unit (Unit 3). Only present at these four sites, Unit 3 is a second <4 m-thick, coralgal reef-dominated unit composed of bindstones, framestones and bafflestones that were deposited in shallow-water, high-energy (0 to 5 m, reef crest-upper slope) setting, except in FPSO-E-C where deeper, more sheltered back reef settings are implied. Ages range from 44 ka to radiocarbon 'dead' and mineralogical data confirm that this reef unit is heavily diagenetically altered, recording extensive mouldic porosity and, in the case of site SWIFT-N1-C, preserving evidence of dolomitization. At the remaining sites WHP, FPSO-SW-C1, FPSO-SW-S1, FPSO-NW-C and SKUA a final distinct unit was observed based on major lithologic, sedimentary facies and mineralogic characteristics. No age data are available for Unit 4 but it is characterised entirely by detrital facies – grainstones, packstones and floatstones that were probably deposited in deeper (>20 m) platforms settings. Mineralogical and SEM data confirm that Unit 4 also was exposed to both marine and meteoric diagenesis (but no evidence of dolomitization was observed).

DISCUSSION

The history of carbonate platform development on the NWS and its relationship to sea-level and associated palaeoenvironmental changes in the region over the past 75 ka is summarised in Fig. 13. After careful sample screening that accounts for their diagenetic characteristics, stratigraphic context and growth position, the nine most reliable NWS RSL data points (including two categorised as less reliable) are shown in Fig. 13A. The authors discuss the implications of the new NWS reef core and bathymetry data in the context of other published sediment core and speleothem records (sediment flux, sea-surface temperature and precipitation) from the region and confirm the NWS is a highly complex submerged landscape characterised by multi-generational carbonate platform structures adjacent to a diverse system of palaeo-shorelines and tidal-estuarine channels. The shallow, internal chrono-stratigraphic structure of platforms records

coherent successions of shallow to deeper reef and platform facies separated by at least two subaerial exposure surfaces that the authors argue reflect the strong control of millennial-scale RSL variability during MIS 4 and MIS 3. Critically, robust U/Th dating of a shallow-water MIS 3 reef unit provides the first constraints on the magnitude of RSL at this time. Apart from a few isolated and distant locations, shallow-water reef development was never re-established regionally on the platforms.

Regional geomorphic interpretation of the submerged landscapes

Initiation and distribution of ICBs in the western Bonaparte Basin has been discussed in detail by Saqab & Bourget (2015). In short, Mesozoic tectonics, associated with Neogene reactivation, controlled the spatial distribution of ICBs by creating palaeotopographic highs in the region. Regionally, reefs were established on these highs during the MIS 15/16 transition as a result of: (1) high-amplitude sea-level fluctuations associated with the reactivation of the carbonate factory during rapid sea-level rises; and (2) drift currents bringing warm, low-salinity and nutrient-rich waters (i.e. Indonesian Throughflow; Gallagher *et al.*, 2014; Gallagher *et al.*, 2017). The combination of these parameters has shaped the 'carbonate palaeolandscape' of the study area. Once established, these carbonate build-ups acted as palaeotopographic highs that facilitated successive phases of carbonate platform growth, including the latest phase(s) of MIS 4-1 development that are the focus of this study.

The 3D seismic imagery has revealed, in unprecedented detail, a range of submerged landscapes both terrestrial and marine in origin (Figs 2 and 3). During lower glacial sea-levels (i.e. MIS 4 and 2) the platform reefs would have featured as low relief topographic highs (i.e. limestone plateaus) above a broad coastal plain (Ishiwa *et al.*, 2016). The shelf to the south of the platform is relatively narrow (8 to 10 km) and orientated towards prevailing SW swells, which dominate the present-day Western Australian coast. This area of shelf probably represented a wave dominated coastal plain with a series of regressive low relief 4 to 8 m-high ridges orientated perpendicular to the SW currently at depths from ~90 to 110 mbsl. Given the ridge orientation they probably formed under a modal SW wave climate.

The shelf seabed NE of the reef platforms exhibits a much more complex but very shallow seaward sloping surface morphology as compared to the shelf located to the SW of the reef platforms (Fig. 2). The north to north-west aspect means the shelf is protected from long period SW swells and therefore would experience a lower energy, possibly tidally dominated environment. The submerged shelf morphology shows a narrowing and termination of channels up against the northern edge of the reef platforms. The channels that deeply incise the reef platforms were probably subject to strong tidal flows during periods of lower sea-level. A complex system of channel and elongate bank features with a distinct absence of narrow meandering channel or oxbow lake morphology also occurs. Both these observations would point to an estuarine-dominated rather than fluvial-dominated coastal plain. Modern examples of such morphologies occur along the Kimberley coast in the Cambridge and Joseph Bonaparte Gulfs (Fig. 1A) and along the southern Gulf of Carpentaria. These active coastal regions are characterised by large estuarine systems dominated by extensive branching tidal channels, mangrove fringed tidal banks and extensive supratidal salt flats. Based on these modern analogues, the elevations of the inter-channel banks should approximate the intertidal zone and therefore provide a relatively narrow indicative range in which to establish a

palaeo-sea-level datum. High-resolution multibeam bathymetry data show tidal bank elevations ranging between -90 and 100 mbsl (Fig. 2). Given this elevation the timing of estuarine development probably occurred during glacial low stands MIS 4 (De Deckker *et al.*, 2019) and MIS 2 (Ishiwa *et al.*, 2019a).

Chrono-stratigraphic results indicate that the NWS reef development occurred during the MIS 3 interstadial, which separates MIS 2 and 4 glacial lowstands (Sections 5.2 to 5.4 for details). Sea-level rise from MIS 4 and into MIS 3 would have resulted in the flooding of these estuarine deposits to a depth of 20 to 30 m. This would be well within wave base of the long period SW swells and may have reworked these higher energy beach ridge sand deposits and the shelf, SW of the reef platforms. Along the lower energy northern shelf the finer sediments, which probably form the tidal channel-bank deposits, may remain undisturbed below a lower energy (shorter wave period) wave base. However, periodic high-energy wave events such as cyclones, or if the region experienced a macrotidal range similar to today, then the reworking/resuspension of these finer estuarine sediments, may have resulted in a more turbid marine environment, potentially impacting or delaying the re-establishment and growth of corals on these reef platforms. The authors lack sufficient age data to evaluate such a lag but the U/Th data confirm shallow-water, high-energy coral reef growth was established by at least 46 ka.

Chrono-stratigraphic interpretation of the units

The NWS drill transects record four chrono-stratigraphic units (Units 1 to 4; Fig. 12) that are defined by internally consistent lithologic, mineralogic, sedimentary facies, reef assemblages and chronologic changes. Fig. 13A shows the NWS platforms have had a complicated evolution over the past 75,000 yr in response to RSL changes operating at different time scales and magnitudes (interstadial/stadial and glacial/interglacial).

As a result, the platforms are characterised by multiple phases of shallow-water, high-energy interstadial-stadial reef growth and deeper-reef slope and platform deposition, bounded by periods of subaerial exposure that are spatially continuous across and between the platforms. The authors' interpretation of multi-generational reef and platform development on the NWS is consistent with other late Pleistocene studies of raised reefs in the Huon Peninsula (Chappell, 2002) and Barbados (Blanchon *et al.*, 2009) on rapidly subsiding submerged reefs in the Huon Gulf and around Hawaii (Webster *et al.*, 2009); and most recently the MIS 3-deglacial GBR shelf edge reefs sampled during IODP Exp. 325 (Gischler *et al.*, 2013; Webster *et al.*, 2018; Yokoyama *et al.*, 2018) that also record short-term, polycyclic reef deposition (and subaerial exposure) in response to precessional (20 ka) and sub-orbital, millennial timescales.

The complex history and internal architecture of the NWS platforms is visualised in Fig. 13A by plotting their probable subsidence pathway (0.2 m kyr^{-1}; Solihuddin *et al.*, 2016) back through time (sloping green rectangle and lines), with the reliable NWS RSL data (red symbols with corresponding palaeo-water depths – Table 6) and other RSL observations from the region. Unit 1 represents a chronologically well constrained period of deep-water, coralline algal-dominated deposition during a brief ~3 kyr period of the late deglacial (see Section 5.5). Unit 2 represents a significant and well constrained ~>10 kyr phase of shallow-water, high-energy coral reef during MIS 3 before its exposure and demise during the RSL fall to the LGM, which is marked by a major palaeosol horizon (see Section 5.3). Unfortunately, the lack of any reliable age

control for Units 3 and 4 make interpretation of their origins difficult. However, several lines of evidence support the interpretation that Unit 3 represents another distinct albeit brief, phase of shallow-water (<5 m) reef development prior to the MIS 4 lowstand ~65 ka (De Deckker *et al.*, 2019). Firstly, its stratigraphic position just below the deeper reef-slope facies at the base of the well-dated MIS 3 reef (Unit 2) represents a major lithologic and paleoenvironmental change (>20 m palaeowater). Secondly, the development of a second major palaeosol horizon marking this boundary (~90 mbsl), combined with Unit 3's more complex mineralogic variations, including significant dolomitization, suggest it had a very different diagenetic history as compared with Unit 2. The euhedral dolomite cement partly replacing high-Mg calcite microbial sediments is consistent with a more complex diagenetic history. Although the dolomite is yet to be studied isotopically, its sporadic nature and occurrence with preserved aragonite and high-Mg calcite are not consistent with the pervasive dolomitization associated with deeper burial or hydrothermal brines (e.g. Drivet & Mountjoy, 1997) or formation in low-energy, evaporative playa-lagoon-sabkha settings (e.g. McKenzie *et al.*, 1980). Its scattered occurrence in reef facies is most consistent with formation during early sea-level fall when mixing between sea water and subordinate freshwater occurred in a phreatic environment (e.g. Machel & Mountjoy, 1986; Strasser & Strohmenger, 1997). However, additional study is required. The authors are unable to tie Unit 3 to a specific sea-level oscillation but the most probable interpretation is that this reef was deposited before the MIS 4 lowstand ~65 ka when the platform was exposed. However, based on uniform regional subsidence rates and its shallow palaeowater depth (<5 m), it is tantalising to speculate that the Unit 3 reef could have developed during a fall in interstadial to stadial RSL, such as MIS 5c to 5b or MIS 5a to 4 (Fig. 13A). Similarly, the age of Unit 4 is unknown but its stratigraphic position (~88 to 106 mbsl) and palaeoenvironment imply that this unit was deposited on non-reefal and deeper (>20 m) platforms during one or more of the higher, interstadial sea-level intervals such as MIS 5a, 5c or less probably MIS 5e. Despite the significant meteoric diagenetic overprint(s) in Units 4 and 3, and less so Unit 2, the hyperspectral, SEM and thin section analyses confirm the presence of original aragonite coral skeleton that could be targeted for fine scale laser ablation-inductively coupled plasma-mass spectrometry to improve chronological constraints.

MIS 3 reef & platform development and palaeoenvironmental changes

The NWS cores define a new record of MIS 3 reef development on the margin (Fig. 13A). Unit 2 represents a significant 10 to 15 m-thick phase of reef development characterised by a distinct shallowing upwards sequence, from deeper fore-reef slope (>20 m water depth) at its base to very shallow, high-energy reef assemblages (<5 m water depth) at the top (Fig. 12A). Unfortunately, no reliable dates are available for the base of this sequence, so the reef turn-on age is unknown. However, U/Th ages confirm that the reef surface was within ~5 m of RSL by ~46 to 39 $\pm$ 0.2 ka, indicating a significant reduction in accommodation (>15 m) and that active vertical reef accretion took place over a sustained interval of MIS 3 time greater than 7 kyr. Environmental conditions must have been optimal for reef development and this is consistent with regional palaeoceanographic data, which indicate relatively warm and stable (~26 to 27°C) SSTs (Zuraida *et al.*, 2009) and comparatively low precipitation (van der Kaars & Deckker, 2002; van der Kaars *et al.*,

2006) and riverine flux (Stuut *et al.*, 2014) during MIS 3 (Fig. 13A).

Shallowing upwards sequences are common features of Quaternary reef systems but their interpretation is far from straightforward. They may result from the simple vertical infilling of accommodation as the reef adopts a 'catch-up' mode of growth from deeper into shallower water or, alternatively, they may be produced as a consequence of lateral reef progradation (see Camoin & Webster, 2015; Braithwaite, 2016 for recent reviews). Core recovery and age control from the NWS sites are insufficient to distinguish between shallowing upwards caused by catch-up growth in response to periods of stable or falling RSL (Fig. 13A) and lateral progradation of the system during MIS 3. However, the consistency of the shallowing upwards patterns within and between the SE and NW core transects, along with the position of most sites at/near the platform margins (Fig. 12B), argues strongly for a vertical shallowing across the platforms, and probably the entire system, over a sustained period of relatively stable sea-level at this position. This is consistent with recent interpretations of many inferred MIS 3 aged and geomorphically mature coastal landscapes (coastal barrier dunes, lagoonal systems, tidal flats and estuarine channels) that have been preserved at similar depths of 70 to 75 mbsl on the outer shelf further south off Barrow and the Montebello Islands (O'Leary *et al.*, 2020) and elsewhere around Australia (Brooke *et al.*, 2017). The NWS cores provide new evidence for extensive coral reef and carbonate platform development on the outer shelf at a similar time.

New record of MIS 3 RSL on the margin; and comparisons with other records

The NWS cores provide new constraints on RSL during MIS 3 along the margin. While there are relatively few reliable ages and given the platforms' complicated growth and exposure history (Section 5.2) in response to repeated and rapid RSL oscillations over the past ~75 ka, the authors interpret the three *in situ*, closed-system U-Th coral dates from the top of Unit 2 to reflect accurately the minimum position of RSL towards the end of MIS 3 (Fig. 13A). These data, along with the authors' palaeowater depth reconstruction (0 to 5 m) and including the modern tidal error, confirm that RSL was between 63 to 75 ± 1.8 mbsl from 45.95 to 39.23 ka $\pm$ 0.2, assuming a similar constant subsidence rate (0.2 mm yr^{-1}) reported for NWS since the LIG (Collins, 2011; Solihuddin *et al.*, 2016). It is acknowledged that by applying a more conservative palaeowater reconstruction of 0 to 10 m, RSL at this time could have been as high as 58 mbsl. Furthermore, RSL could have been even higher if the authors' interpretation was incorrect that only a little material was eroded away (i.e. is a significant section missing?) during subsequent subaerial exposure and palaeosol formation at the top of the platform when RSL fell to MIS 2 some time after ~30 ka. However, based on interpretation of similar styles of palaeosol formation observed at the top of the LIG (Dechnik *et al.*, 2017) and MIS 3 (Gischler *et al.*, 2013) GBR deposits, the authors consider this improbable. It is also not probable that significant erosion would have occurred during the deglacial reflooding stage, given the level of lithification/ cementation observed in reef Unit 2.

These uncertainties aside, the authors' preferred NWS constraints (63 to 75 ± 1.8 mbsl from 45.95 to 39.23 $\pm$ 0.2 ka) are broadly consistent with recent RSL predictions for the region (Ishiwa *et al.*, 2019a) and observations from reef terraces at the Huon Peninsula (see Hibbert *et al.*, 2016 for original data sources and a new compilation). The authors' data also support recent published observations and models of Northern Hemisphere ice sheets (Carlson *et*

al., 2018; Pico *et al.*, 2018; Dalton *et al.*, 2019) that indicate higher ESLs during MIS 3 than previously thought, based on other records such as the Red Sea isotope record (Grant *et al.*, 2012). The authors acknowledge that there are currently inadequate reliable dates from the NWS cores to constrain MIS 3 RSL further or to accurately date the end of MIS 3. However, they do represent important new MIS 3 RSL reference points with which to connect to the new history of MIS 2 sea-level variations recorded in Bonaparte Gulf sediment cores (Ishiwa *et al.*, 2019a; Fig. 1A). Together the cores imply a drop in RSL of >40 m following the end of MIS 3 to the start of the sea-level plateau at ~26 ka at ~110 mbsl, that preceded the MIS 2 minimum of ~19.7 to 19.1 ka.

Why did the shallow coral reefs fail to re-establish during deglacial-MIS 1?

Core data confirm that shallow-water coral development was unable to re-establish itself as sea-level reflooded the tops of the platforms during the deglacial. Rather, between ~13.2 and 10.7 ka deposition on the platforms was dominated by a relatively thin (~1 m) veneer of deeper, reef slope rhodolith facies (Unit 1). This facies is similar to modern rhodolith habitats that occur in water depths of >20 to 45 mbsl on the tops of adjacent banks and shoals (Barracouta and Vulcan; Heyward *et al.*, 2010), banks further to the north (Van Diemem's Rise; Anderson *et al.*, 2011) and deep fore-reef slopes to the south (Helby Bank and Osprey; Turner *et al.*, 2018). This is entirely consistent with the interpretation that they were deposited in water depths >20 m (Fig. 13A) and is supported by their common occurrence in the latter stages of coral reef and platform drowning in Late Quaternary reefs system around the world (see Webster *et al.*, 2009 for a summary). However, in case of the NWS, based on observations from drill transects, this deep-water facies was deposited directly on top of the subaerial exposure surface marking the demise of the MIS 3 reef unit.

No data are available for the adjacent Ashmore Reef, which grew to present sea-level. However, drilling data from Scott Reef further to the south (Fig. 1A) indicate that reef development occurred from 11.5 ka at a depth of 58 mbsl (Collins *et al.*, 2011). Whilst the authors cannot preclude the existence of shallow-water reef grow at depths between 60 and 75 m, these data raise the obvious question as to why reef development was not able to re-establish itself over a huge >700 km by 300 km region of available substrate provided by the older, MIS 3 reef platforms. Fig. 13C shows the seabed <80 mbsl that roughly estimates the maximum extent of any MIS 3 reefs and carbonate platform systems that would have been available substrates for subsequent deglacial-Holocene reef development. With exception of a select few reefs on the NWS (i.e. Ashmore, Cartier, Scott and Adele reefs) that re-established and were able to 'keep up' or 'catch up' to present sea-level, the authors argue that the combination of the depth of the NWS platforms at ~75 to 80 mbsl, the rate of RSL rise and poor water quality caused by the massive, influx of riverine sediments and/or sediment remobilisation at the time were what impeded reef growth in most areas. These factors are discussed in turn below.

Based on their depths and comparisons with RSL data from the Bonaparte Gulf (Ishiwa *et al.*, 2019a), the NWS platforms would probably have been reflooded by ~14 to 15 ka (Fig. 13A). This is consistent with RSL reconstructions from Sunda Shelf and Tahiti that indicate rapid sea-level rise (40 to 50 mm yr^{-1}), including the meltwater pulse event 1A (MWP-1A) at this time (Hanebuth *et al.*, 2000; Deschamps *et al.*, 2012). Furthermore, IODP Exp. 325 drilling on the GBR, while unable to provide improved constraints on MWP-1A, indicated rapid

RSL rise during this mid-deglacial (~16 to 13 ka) on the order of 20 to 60 mm yr^{-1} (Yokoyama *et al.*, 2018). Therefore, at this crucial time/depth the rate and magnitude of platform flooding may have been too rapid to allow initiation and sustained development of shallow-water reefs. However, significantly, the authors' geomorphic analysis reveals that the NWS platform tops become increasingly shallow if considering a transect towards Ashmore Reef. This implies a classical backstepping of the platform with the final expression of catch-up being Ashmore Reef and Cartier Island, despite the former being rimmed by an extensive sequence of drowned terraces between 70 to 30 mbsl (Glenn *et al.*, 2007). Thus, some other factor(s), perhaps related to their more oceanic and distal position on the outer shelf, may have allowed these few NWS reefs (including Scott and Adele) to reach present level.

The authors' review of the relevant palaeoenvironmental proxy records for the NWS (Fig. 13B) provides additional evidence that, in contrast to MIS 3, oceanographic conditions during the mid-late deglaciation were far from optimal for coral reef development. Land-based speleothems and marine sediment pollen records along the margin confirm that precipitation was very high during the mid-deglacial to the early Holocene (~15 to 8.5 ka; van der Kaars & Deckker, 2002; van der Kaars *et al.*, 2006; Denniston *et al.*, 2013). This is consistent with numerous deep sea marine sediment cores in the region that record a massive increase in riverine sediment input during that period (Stuut *et al.*, 2014; Kuhnt *et al.*, 2015) as a result of a major strengthening of the ASM caused by the southern migration of the Intertropical Convergence Zone (ITCZ; Kuhnt *et al.*, 2015; Ishiwa *et al.*, 2019b).

Significant palaeo-rivers in the region (i.e. palaeo-Fitzroy and Ord rivers, Fig. 1A) may have acted as major sources of riverine sediment at that time. Apart from enhanced riverine input, other oceanographic factors may have contributed to enhanced sediment flux via the resuspension of shelf sediments. For example, numerous large sediment waves, contourites and channels occur along the NWS between 55 to 130 m, where the sea floor may have experienced stronger bottom currents influenced by different internal waves, tides and storms during the mid-deglaciation (16.0 ka and 13.3 ka; Bischoff, 2014; Belde *et al.*, 2017). Poor water quality due to elevated sediment and nutrient flux has been implicated in the degradation and demise of numerous deglacial and Holocene reefs around the world (e.g. Montaggioni, 2005; Gischler, 2015; Webster *et al.*, 2018), but on the NWS it may have impeded re-establishment of shallow-water reef growth on the platforms during deglacial reflooding.

Regardless of which factor(s) (RSL rise rate *vs*. water quality) was most important, compared with the previous phase of high-energy, shallow-water coral reef during MIS 3, the lack of shallow-water reef growth during MIS 1 represents a major hiatus in platform building across the NWS. Excepting a few isolated reefs that were able to reach present sea-level, this vast network of submerged banks and shoals now provide highly important and diverse modern mesophotic reef habitats (Heyward, 1997; Anderson *et al.*, 2011; Moore *et al.*, 2017).

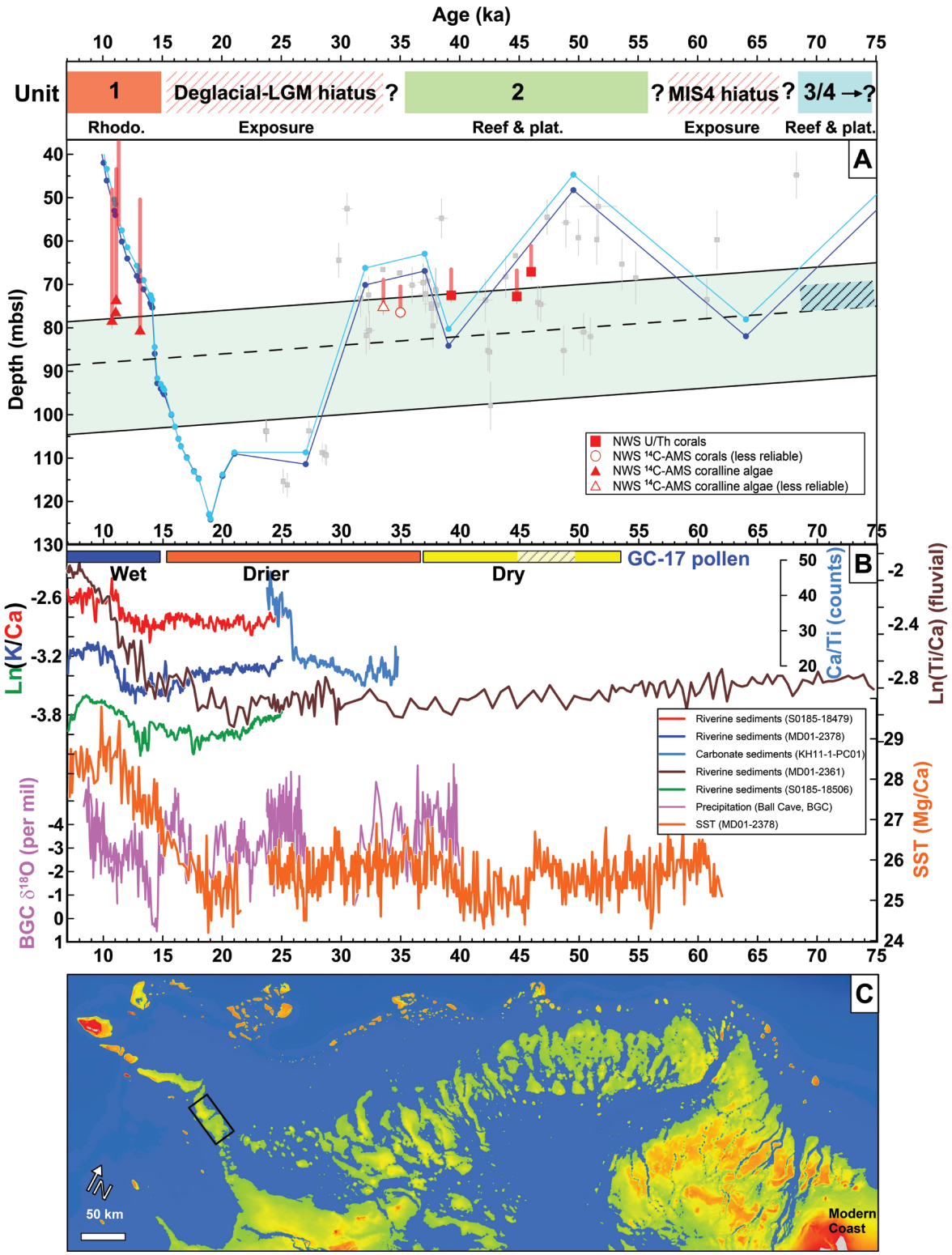

Fig. 13. Summary of the most reliable RSL observations, reef and platform development and relevant palaeoceanographic proxies from the NWS from MIS 4-1. (A) Age versus depth of reliable U/Th and ^{14}C-AMS dates, their relationship with predicted regional RSL (dark blue) and ESL (light blue) (Ishiwa *et al.*, 2019a) as well as regional subsidence (sloping green rectangle and lines) (Solihuddin *et al.*, 2016). The elevations of the NWS RSL data are corrected for regional subsidence and of the samples with paired ^{14}C-

AMS and U/Th ages only the U/Th is plotted (see Table 5). Palaeo-water depths based on reef biotic assemblages are indicated by the vertical red bars. Age and tidal uncertainties are shown or smaller than the plotted symbols. The sloping green rectangle and lines represents the probable subsidence pathway of key platform and chrono-stratigraphic unit depths (-80, -90 (dashed) and -106 mbsl). The temporal distribution of chrono-stratigraphic units (1 to 4) and their interpreted corresponding depositional stage and environment is also shown. The hatched blue rectangle represents one possible depositional depth and time of reef Unit 3; that was subsequently exposed during MIS 4 and then again during MIS 2. RSL coral data (grey squares) from the Huon Peninsula spanning MIS 3-2 are also shown (see Hibbert *et al*., 2016 original data sources). (B) Summary of relevant palaeoenvironmental proxy records for the NWS over the past 75,000 yr. See Fig. 1A for the locations of the marine sediment cores recording regional sea-surface temperatures (SST) (Zuraida *et al*., 2009; Sarnthein *et al*., 2011), riverine sediment input (Stuut *et al*., 2014; Kuhnt *et al*., 2015), carbonate sediment input (Ishiwa *et al*., 2016), pollen composition indicating wet *vs*. dry periods (van der Kaars & Deckker, 2002; van der Kaars *et al*., 2006) and land-based speleothems (Denniston *et al*., 2013) as a proxy for precipitation. Note the wet conditions and high regional, riverine input during from ~15 to 8.5 ka. (C) Visualisation showing the approximate position of the shoreline at 80 mbsl based on an extraction (>80 m blue pixels) of the available bathymetric data (Beaman, 2018) and the detailed study site (black rectangle). The green pixels represent the maximum extent of the reef and carbonate platform system that was growing during MIS 4-3 before being terminated by sea-level fall to MIS 2. Apart from the most offshore areas (Ashmore, Cartier, Adele and Scott Reefs) significant shallow-water coral reef development, at or near sea-level, was never re-established on the majority of these platforms during deglaciation and MIS 1. The position of the modern coastline relative to this -80 m shoreline visualisation is shown in grey (bottom right – Melville Island) and in Fig. 1A.

CONCLUSIONS

The NWS cores, combined with seabed geomorphology data, constrain the history of platform and shelf development as well as sea-level changes over the past 50,000 yr. The authors conclude that:

(1) The 3D seismic-derived and multibeam bathymetry datasets record a complex submerged landscape shaped by changes in sea-level, sediment input and transport pathways, together with carbonate platform development through MIS 4 to 1. Three distinct, multigenerational platforms occur between ~80 to 60 mbsl; these are rimmed semi-continuously by smaller reef terraces and bisected by deeper channels. A succession of linear palaeo-shoreline features to the SW and a complex tidal-estuarine channel system to the NE are interpreted to have formed at lower sea-levels (>90 to 110 m) during MIS 2 and 4 when the platform was exposed.

(2) The two drill transects record four chrono-stratigraphic units (Units 1 to 4) that are defined by internally consistent lithologic, mineralogic, sedimentary facies, reef assemblages and chronologic changes. Despite some missing sections, these units can be correlated up to 17 km between transects and sites at depths of ~75 and 106 mbsl; and reflect a wide range of shallow to deep depositional reef and platform settings.

(3) Chronologic data (^{14}C-AMS, U/Th ages) confirm episodic platform development that spans 10.7 to >50 ka. Repeated facies successions deposited in very shallow, high-energy reef (<5 m) and deeper fore reef slope settings (>20 m), along with clear evidence of meteoric diagenetic alteration (including two palaeosol intervals at ~80 and 90 mbsl and dolomitization at 90 to 92 mbsl in Unit 3) reflect the complex pattern of platform growth and demise (exposure) in response to repeated sea-level fluctuation from MIS 4 to MIS 1.

(4) The authors define a significant 10 to 15 m-thick coral reef-dominated phase of platform development (Unit 2) during MIS 3.

Constrained by the first reliable, closed-system U/Th ages (45.95 to 39.23 ± 0.2 ka) on the NWS, this unit records a clear shallowing upwards sequence based on reef assemblages before subaerial exposure and demise as sea-level fell to the LGM towards the end of MIS 3 ~30 ka. The age of an older, diagenetically distinct reef unit (Unit 3) is unknown but is interpreted to have developed prior to the MIS 4 lowstand ~65 ka.

(5) The NWS chronologic and palaeowater data confirm that the RSL was between ~63 to 75 ± 1.8 mbsl during MIS 3 (45.95 to 39.23 ± 0.2 ka), consistent with RSL predictions for the region and uplifted reef terraces on the Huon Peninsula. This also supports recently published observations and models of Northern Hemisphere ice sheets indicating higher ESLs during MIS 3.

(6) The platform system was unable to fully re-establish itself following reflooding during the deglacial sea-level rise. Deeper reef slope (Unit 1) facies dominate the core tops between ~13.2 to 10.7 ka, representing a major hiatus in shallow-water reef development on the platform. Unlike other margins around the world, deglacial sea-level rise was either too fast and/or other environmental conditions were unfavourable (i.e. massive riverine sediment flux due the changing monsoon and/or resuspension of shelf sediments) to allow re-establishment of shallow water coral reef development apart from on a few isolated and more distal locations (i.e. Ashmore, Cartier, Adele and Scott Reefs). The more distal locations of those reefs may provide support for the adverse water quality hypothesis on the more inshore platforms.

ACKNOWLEDGEMENTS

We thank the PTTEP Australasia for recovering the cores from the NWS and we acknowledge Dr. Alisha Thompson and Wenona School (Sydney, NSW) for the use of their SEM facilities. Financial support for this research was provided by the Australian Research Council (grants DP1094001, DP120101793). We thank Geoscience Australia for providing the 3D seismic data and Eliis for providing the PaleoScan™ software.

REFERENCES

Abbey, E., Webster, J.M., Braga, J.C., Sugihara, K., Wallace, C., Iryu, Y., Potts, D., Done, T., Camoin, G. and **Seard, C.** (2011) Variation in deglacial coralgal assemblages and their paleoenvironmental significance: IODP Expedition 310, "Tahiti Sea Level". *Global Planet. Change*, **76**, 1–15.

Abdul, N.A., Mortlock, R.A., Wright, J.D. and **Fairbanks, R.G.** (2016) Younger Dryas Sea-Level and Meltwater Pulse 1B Recorded in Barbados Reef-Crest Coral Acropora palmata. *Paleoceanography*, **31**, 330–344.

Adey, W.H., Townsend, R.A. and **Boykins, W.T.** (1982) The crustose coralline algae (Rhodophyta: Corallinaceae) of the Hawaiian Islands. *Smithson. Contrib. Mar. Sci*., **15**, 1–74.

Anderson, T., Scott Nichol, L.R., Heap, A.D., Battershill, C., Hughes, M., Vaughn Barrie, P.J.S., Alvarez de Glasby, B., Tran, M., Daniell, J. and **Shipboard Party** (2011) *Seabed Environments of the Eastern Joseph Bonaparte Gulf, Northern Australia*, Aust. Inst. Mar. Sci., 61 pp.

Apthorpe, M.C. (1988) Cainozoic Depositional History of the North West Shelf. In: *The North West Shelf, Australia Symposium* (Eds P.G. Purcell and R.R. Purcell), 1988-08-10, The Petroleum Exploration Society of Australia (PESA), Perth, pp. 55–84.

Australian Hydrographic Office (2018) *Tide Predictions for Australia*.

Bassi, D., Iryu, Y. and **Nebelsick, J.H.** (2012) To Be or Not to Be a Fossil Rhodolith? Analytical Methods for Studying Fossil Rhodolith Deposits. *J. Coastal Res*., **279**, 288–295.

Beaman, R.J. (2018) *High-resolution depth model for Northern Australia - 100 m*. James Cook University, Cairns, Australia. Available at: https://www.deepreef.org/bathymetry/219-nthaus-bathy.html.

Belde, J., Reuning, L. and **Back, S.** (2017) Bottom currents and sediment waves on a shallow carbonate shelf, Northern Carnarvon Basin, Australia. *Cont. Shelf Res*., **138**, 142–153.

Berry, P.E. (1993) Historical background, description of the physical environments of Ashmore Reef and Cartier Island and notes on exploited species. *Records of the Western Australian Museum Supplement*, **44**, 1–11.

Bird, M.I., Beaman, R.J., Condie, S.A., Cooper, A., Ulm, S. and **Veth, P.** (2018) Palaeogeography and voyage modeling indicates early human colonization of Australia was likely from Timor-Roti. *Quatern. Sci. Rev*., **191**, 431–439.

Bischoff, K. (2014) *Controls on the stratigraphic evolution of an isolated carbonate buildup setting: Quaternary example from the Timor Sea (NW Australia)*. The University of Western Australia, 93 pp.

Blanchon, P., Eisenhauer, A., Fietzke, J. and **Liebetrau, V.** (2009) Rapid sea-level rise and reef back-stepping at the close of the last interglacial highstand. *Nature*, **458**(7240), 881–884.

Bourget, J., Ainsworth, R.B., Backé, G. and **Keep, M.** (2012) Tectonic evolution of the northern Bonaparte Basin: impact on continental shelf architecture and sediment distribution during the Pleistocene. *Aust. J. Earth Sci*., **59**(6), 877–897.

Bradshaw, M.T., Yeates, A.N., Beynon, R.M., Brakel, A.T., Langford, R.P., Totterdell, J.M. and **Yeung, M.** (1988) Paleogeographic evolution of the North West shelf region; Evolution paléogéographique de la région de la plateforme nord-occidentale australienne, The North West Shelf, Australia Symposium, 1988-08-10, The Petroleum Exploration Society of Australia (PESA), Perth, pp. 29–54.

Braga, J.C., Humblet, M., Ramos, D.A.E., Dechnik, B. and Webster, J.M. Quaternary coral, coralline algal and vermetid assemblages as sea-level indicators: a review. In: *Coral Reefs and Sea-Level Change: Quaternary Records and Modelling. A Window Into the Future* (Eds G.F. Camoin and N. Hallmann), *Int. Assoc. Sedimentol. Spec. Publ*., **49** (this volume), 1–38.

Braithwaite, C.J.R. (2016) Coral-reef records of Quaternary changes in climate and sea-level. *Earth-Sci. Rev*., **156**, 137–154.

Braithwaite, C.J.R. and **Montaggioni, L.F.** (2009) The Great Barrier Reef: a 700,000 year diagenetic history. *Sedimentology*, **56**(6), 1591–1622.

Brooke, B.P., Nichol, S.L., Huang, Z. and **Beaman, R.J.** (2017) Palaeoshorelines on the Australian continental shelf: Morphology, sea-level relationship and applications to environmental management and archaeology. *Cont. Shelf Res*., **134**, 26–38.

Budd, A.F., Fukami, H., Smith, N.D. and **Knowlton, N.** (2012) Taxonomic classification of the reef coral family Mussidae (Cnidaria: Anthozoa: Scleractinia). *Zool. J. Linn. Soc*., **166**(3), 465–529.

Cabioch, G., Montaggioni, L.F., Faure, G. and **Ribaud-Laurenti, A.** (1999) Reef coralgal assemblage as recorders of paleobathymetry and sea level changes in the Indo-Pacific province. *Quatern. Sci. Rev*., **18**, 1681–1695.

Cadman, S.J. and **Temple, P.R.** (2004) Bonaparte Basin, NT, WA, AC & JPDA. *Australian Petroleum Accumulations Report*, **5**, Geoscience Australia, Canberra.

Camoin, G.F., Iryu, Y., McInroy, D.B. and **Scientists, E.** (2007) Proceedings of the Integrated Ocean Drilling Program Volume 310 Expedition Reports Tahiti Sea Level. *Proceedings of the Integrated Ocean Drilling Program*, **310**, doi:10.2204/iodp.proc.310.101.2007.

Camoin, G.F., Seard, C., Deschamps, P., Webster, J.M., Abbey, E., Braga, J.C., Iryu, Y., Durand, N., Bard, E., Hamelin, B., Yokoyama, Y., Thomas, A.L., Henderson, G.M. and **Dussouillez, P.** (2012) Reef response to sea-level and environmental changes during the last deglaciation: Integrated Ocean Drilling Program Expedition 310, Tahiti Sea Level. *Geology*, **40**(7), 643–646.

Camoin, G.F. and **Webster, J.M.** (2015) Coral reef response to Quaternary sea-level and environmental changes: State of the science. *Sedimentology*, **62**(2), 401–428.

Carlson, A.E., Tarasov, L. and **Pico, T.** (2018) Rapid Laurentide ice-sheet advance towards southern last glacial maximum limit during marine isotope stage 3. *Quatern. Sci. Rev*., **196**, 118–123.

Ceccarelli, D.M., Richards, Z.T., Pratchett, M.S. and **Cvitanovic, C.** (2011) Rapid increase in coral cover on an isolated coral reef, the Ashmore Reef National Nature Reserve, north-western Australia. *Mar. Freshw. Res.*, **62**(10).

Chappell, J. (2002) Sea level changes forced ice breakouts in the Last Glacial cycle: new results from the coral terraces. *Quatern. Sci. Rev*., **21**(10), 1229–1240.

Cheng, H., Edwards, R.L., Hoff, J., Gallup, C.D., Richards, D.A. and **Asmerom, Y.** (2000) The half-lives of uranium-234 and thorium-230. *Chem. Geol*., **169**(1), 17–33.

Chutcharavan, P.M., Dutton, A. and **Ellwood, M.J.** (2018) Seawater 234U/238U recorded by modern and fossil corals. *Geochim. Cosmochim. Acta*, **224**, 1–17.

Clark, T.R., Roff, G., Zhao, J.-x., Feng, Y.-x., Done, T.J. and **Pandolfi, J.M.** (2014) Testing the precision and accuracy of the U–Th chronometer for dating coral mortality events in the last 100 years. *Quatern. Geochronol*., **23**, 35–45.

Collins, L.B. (2011) Geological Setting, Marine Geomorphology, Sediments and Oceanic Shoals Growth History of the Kimberley Region. *J. Roy. Soc. W. Aust*., **94**, 89–105.

Collins, L.B., Testa, V., Zhao, J. and **Qu, D.** (2011) Holocene Growth History and Evolution of the Scott Reef Carbonate Platform and Coral Reef. *J. Roy. Soc. W. Aust*., **94**, 239–250.

CoralTraitDatabase (2020) Coral Trait Database. https://coraltraits.org/

Cutler, K.B., Edwards, R.L., Taylor, F.W., Cheng, H., Adkins, J., Gallup, C.D., Cutler, P.M., Burr, G.S. and **Bloom, A.** (2003) Rapid sea-level fall and deep-ocean temperature change since the last interglacial period. *Earth Planet. Sci. Lett*., **206**, 253–271.

Dalton, A.S., Finkelstein, S.A., Forman, S.L., Barnett, P.J., Pico, T. and **Mitrovica, J.X.** (2019) Was the Laurentide Ice Sheet significantly reduced during Marine Isotope Stage 3? *Geology*, **47**(2), 111–114.

De Deckker, P., Arnold, L.J., van der Kaars, S., Bayon, G., Stuut, J.-B.W., Perner, K., Lopes dos Santos, R., Uemura, R. and **Demuro, M.** (2019) Marine Isotope Stage 4 in Australasia: A full glacial culminating 65,000 years ago – Global connections and implications for human dispersal. *Quatern. Sci. Rev*., **204**, 187–207.

Dechnik, B., Webster J. M., Davies, P.J., Braga, J.C. and **Reimer, P.J.** (2015) Holocene 'turn-on' and evolution of the Southern Great Barrier Reef: Revisiting reef cores from the Capricorn Bunker Group. *Mar. Geol*., **363**, 174–190.

Dechnik, B., Webster, J.M., Webb, G.E., Nothdurft, L., Dutton, A., Braga, J.-C., Zhao, J.-x., Duce, S. and **Sadler, J.** (2017) The evolution of the Great Barrier Reef during the Last Interglacial Period. *Global Planet. Change*, **149**, 53–71.

Denniston, R.F., Wyrwoll, K.-H., Asmerom, Y., Polyak, V.J., Humphreys, W.F., Cugley, J., Woods, D., LaPointe, Z., Peota, J. and **Greaves, E.** (2013) North Atlantic forcing of millennial-scale Indo-Australian monsoon dynamics during the Last Glacial period. *Quatern. Sci. Rev*., **72**(0), 159–168.

Deschamps, P., Durand, N., Bard, E., Hamelin, B., Camoin, G., Thomas, A.L., Henderson, G.M., Okuno, J.i. and **Yokoyama, Y.** (2012) Ice-sheet collapse and sea-level rise at the Bølling warming 14,600 years ago. *Nature*, **483**(7391), 559–564.

Drivet, E. and **Mountjoy, E.W.** (1997) Dolomitization of the Leduc Formation (Upper Devonian), southern Rimbey-Meadowbrook reef trend, Alberta. *J. Sed. Res*., **67**(3), 411–423.

Dutton, A., Carlson, A.E., Long, A.J., Milne, G.A., Clark, P.U., DeConto, R., Horton, B.P., Rahmstorf, S. and **Raymo, M.E.** (2015) Sea-level rise due to polar ice-sheet mass loss during past warm periods. *Science*, **349**(6244), aaa4019.

Dutton, A. and **Lambeck, K.** (2012) Ice Volume and Sea Level During the Last Interglacial. *Science*, 337 (6091), 216–219, DOI: 10.1126/science.1205749.

Fairbanks, R.G., Mortlock, R.A., Chiu, T.-C., Cao, L., Kaplan, A., Guilderson, T.P., Fairbanks, T.W., Bloom, A.L., Grootes, P.M. and **Nadeau, M.-J.** (2005) Radiocarbon calibration curve spanning 0 to 50,000 years BP based on paired 230Th/234U/238U and 14C dates on pristine corals. *Quatern. Sci. Rev*., **24**(16-17), 1781–1796

Gallagher, S.J., Fulthorpe, C.S., Bogus, K.A. and **Scientists, E.** (2017) Expedition 356 Summary. *Proceedings of the International Ocean Discovery Program*, **356**, 43 pp.

Gallagher, S.J., Wallace, M.W., Hoiles, P.W. and **Southwood, J.M.** (2014) Seismic and stratigraphic evidence for reef expansion and onset of aridity on the Northwest Shelf of Australia during the Pleistocene. *Mar. Petrol. Geol*., **57**, 470–481.

Gallagher, S.J., Wallace, M.W., Li, C.L., Kinna, B., Bye, J.T., Akimoto, K. and **Torii, M.** (2009) Neogene history of the West Pacific Warm Pool, Kuroshio and Leeuwin currents. *Paleoceanography*, **24**(1), 1–27.

Gentilli, J. (1972) Australian Climate Patterns. Thomas Nelson, Melbourne, 285 pp.

Gischler, E. (2015) Quaternary reef response to sea-level and environmental change in the western Atlantic. *Sedimentology*, **62**(2), 429–465.

Gischler, E., Hudson, H.J., Humblet, M., Braga, J.C., Eisenhauer, A., Isaack, A., Anselmetti, F.S. and **Camoin, G.F.** (2016) Late Quaternary barrier and fringing reef development of Bora Bora (Society Islands, south Pacific): first subsurface data from Darwin's type barrier-reef system. *Sedimentology*, 1522–1549.

Gischler, E., Thomas, A.L., Droxler, A.W., Webster, J.M., Yokoyama, Y., Schöne, B.R. and **Porta, G.D.** (2013) Microfacies and diagenesis of older Pleistocene (pre-last glacial maximum) reef deposits, Great Barrier Reef, Australia (IODP Expedition 325): A quantitative approach. *Sedimentology*, **60**, 1432–1466.

Glenn, K.C. (2004) *Sedimentary processes during the Late Quaternary across the Kimberley Shelf, Northwest Australia*. PhD Thesis, The University of Adelaide, 266 pp.

Glenn, K.C., Beard, M. and **Pisel., S.** (2007) *Ashmore Reef: from Lead line to LADS*.

Glenn, K.C. and **Collins, D.** (2005) Ashmore Reefs sedimentologic and morphological response to sea level rise. *The Beagle, Records of the Museums and Art galleries of the Northern Territory Supplement*, **1**, 13–29.

Gordon, A.L. (2005) Oceanography of the Indonesian Seas and the throughflow. *Oceanography*, **4**, 14–27.

Gowan, E.J., Zhang, X., Khosravi, S., Rovere, A., Stocchi, P., Hughes, A.L.C., Gyllencreutz, R., Mangerud, J., Svendsen, J.I. and **Lohmann, G.** (2021) A new global ice sheet reconstruction for the past 80 000 years. *Nature Comms*, **12**(1), 1199.

Grant, K.M., Rohling, E.J., Bar-Matthews, M., Ayalon, A., Medina-Elizalde, M., Ramsey, C.B., Satow, C. and **Roberts, A.P.** (2012) Rapid coupling between ice volume and polar temperature over the past 150,000 years. *Nature*, **491**(7426), 744–747.

Gunn, P.J. (1988) Bonaparte Basin: evolution and structural framework. . In: P.G. Purcell and R.R. Purcell (Editors), The North West shelf, Australia. Symposium 1988-08-10, The Petroleum Exploration Society of Australia (PESA), Perth, 275–285.

Hanebuth, T., Stattegger, K. and **Grootes, P.M.** (2000) Rapid Flooding of the Sunda Shelf: A Late-Glacial Sea-Level Record. *Science*, **288**(5468), 1033–1035.

Heyward, A., Moore, C., Radford, B. and **Colquhoun, J.** (2010) Monitoring Program for the Montara Well Release Timor Sea: Final Report on the Nature of Barracouta and Vulcan Shoals. Report prepared by the *Australian Institute of Marine Science* for PTTEP Australasia (Ashmore Cartier) Pty. Ltd.

Heyward, A., Pinceratto, E. and **Smith, L.** (1997) Big Bank Shoals of the Timor sea: an environmental resource atlas. Australian Institute of Marine Science and BHP Petroleum, Townsville, 115 pp.

Hibbert, F.D., Rohling, E.J., Dutton, A., Williams, F.H., Chutcharavan, P.M., Zhao, C. and **Tamisiea, M.E.** (2016) Coral indicators of past sea-level change: A global repository of U-series dated benchmarks. *Quatern. Sci. Rev.*, **145**, 1–56.

Hirabayashi, S., Yokoyama, Y., Suzuki, A., Miyairi, Y. and **Aze, T.** (2017) Short-term fluctuations in regional radiocarbon reservoir age recorded in coral skeletons from the Ryukyu Islands in the north-western Pacific. *J. Quatern. Sci.*, **32**(1), 1–6.

Huang, D., Arrigoni, R., Benzoni, F., Fukami, H., Knowlton, N., Smith, N.D., Stolarski, J., Chou, L.M. and **Budd, A.F.** (2016) Taxonomic classification of the reef coral family Lobophylliidae (Cnidaria: Anthozoa: Scleractinia). *Zool. J. Linn. Soc*., **178**(3), 436–481.

Huang, D., Benzoni, F., Fukami, H., Knowlton, N., Smith, N.D. and **Budd, A.F.** (2014) Taxonomic classification of the reef coral families Merulinidae, Montastraeidae and Diploastraeidae (Cnidaria: Anthozoa: Scleractinia). *Zool. J. Linn. Soc*., **171**(2), 277–355.

Humblet, M., Hongo, C. and **Sugihara, K.** (2015) An identification guide to some major Quaternary fossil reef-building coral genera (Acropora,Isopora,Montipora, andPorites). *Island Arc*, **24**(1), 16–30.

Humblet, M., Potts, D.C., Webster, J.M., Braga, J.C., Iryu, Y., Yokoyama, Y., Bourillot, R., Séard, C., Droxler, A., Fujita, K., Gischler, E. and **Kan, H.** (2019) Late glacial to deglacial variation of coralgal assemblages in the Great Barrier Reef, Australia. *Global Planet. Change*, **174**, 70–91.

Humblet, M. and **Webster, J.M.** (2017) Coral community changes in the Great Barrier Reef in response to major environmental changes over glacial-interglacial timescales. *Palaeogeogr. Palaeoclimatol. Palaeoecol*., **472**, 216–235.

Iryu, Y., Nakamori, T., Matsuda, S. and **Abe, O.** (1995) Distribution of marine organisms and its geological significance in the modern reef complex of the Ryukyu Islands. *Sed. Geol*., **99**(3-4), 243–258.

Ishiwa, T., Yokoyama, Y., Miyairi, Y., Ikehara, M. and **Obrochta, S.** (2016) Sedimentary environmental change induced from late Quaternary sea-level change in the Bonaparte Gulf, northwestern Australia. *Geosci. Lett*., **3**(1).

Ishiwa, T., Yokoyama, Y., Okuno, J., Obrochta, S., Uehara, K., Ikehara, M. and **Miyairi, Y.** (2019a) A sea-level plateau preceding the Marine Isotope Stage 2 minima revealed by Australian sediments. *Sci. Rep*., **9**(1), 6449. DOI:10.1038/s41598-019-42573-4.

Ishiwa, T., Yokoyama, Y., Reuning, L., McHugh, C.M., De Vleeschouwer, D. and **Gallagher, S.J.** (2019b) Australian Summer Monsoon variability in the past 14,000 years revealed by IODP Expedition 356 sediments. *Prog. Earth Planet. Sci*., **6**(1).

James, N.P., Bone, Y., Kyser, T.K., Dix, G.R. and **Collins, L.B.** (2004) The importance of changing oceanography in controlling late Quaternary carbonate sedimentation on a high-energy, tropical, oceanic ramp: north-western Australia. *Sedimentology*, **51**(6), 1179–1205.

Keep, M. and **Haig, D.W.** (2010) Deformation and exhumation in Timor: Distinct stages of a young orogeny. *Tectonophysics*, **483**(1), 93–111.

Kiessling, W., Simpson, C., Beck, B., Mewis, H. and **Pandolfi, J.M.** (2012) Equatorial decline of reef corals during the last Pleistocene interglacial. *Proc. Natl. Acad. Sci. USA*, **109**(52), 21378–21383.

Kordi, M.N. and **O'Leary, M.** (2016) Geomorphic classification of coral reefs in the north western Australian shelf. *Regional Studies in Marine Science*, **7**, 100–110.

Kospartov, M., Beger, M., Ceccarelli, D.M. and **Richards, Z.T.** (2006) *An assessment of the distribution and abundance of sea cucumbers trochus giant clams coral fish and invasive marine species at Ashmore reef national nature reserve and Cartier island marine reserve: 2005, The Department of Environment and heritage*. Report issued by the Department of the Environment and Heritage, Canberra, 298 pp.

Kuhnt, W., Holbourn, A., Xu, J., Opdyke, B., De Deckker, P., Röhl, U. and **Mudelsee, M.** (2015) Southern Hemisphere control on Australian monsoon variability during the late deglaciation and Holocene. Nat Commun, **6**, 5916.

Longley, I.M., Buessenschuett, C., Clydsdale, L., Cubitt, C.J., Davis, R.C., Johnson, M.K., Marshall, N.M., Murray, A.P., Somerville, R., Spry, T.B. and **Thompson, N.B.** (2002) The North West Shelf of Australia - a Woodside perspective. . In: S.J. Moss and M. Keep (Editors), The sedimentary basins of Western Australia 3. Petroleum Exploration Society of Australia., pp. 27–88.

Ludwig, K. (2012) *Isoplot 3.75–4.15: a geochronological toolkit for Microsoft Excel*. Berkeley Geochronology Center Special Publication. Berkeley, California, 75 pp.

Lund, M.J., Davies, P.J. and **Braga, J.C.** (2000) Coralline algal nodules off Fraser Island, eastern Australia. *Facies*, **42**, 25–34.

Machel, H.-G. and **Mountjoy, E.W.** (1986) Chemistry and Environments of Dolomitization - A Reappraisal. *Earth-Sci. Rev.*, **23**(3), 175–222.

Marshall, N.G. and **Lang, S.C.** (2013) A new sequence stratigraphic framework for the North West Shelf, Australia. . In: *The Sedimentary Basins of Western Australia 4* (Eds M. Keep and S.J. Moss), *Proceedings of the Petroleum Exploration Society of Australia Symposium*, pp. 1–31.

Matsuda, S. and **Iryu, Y.** (2011) Rhodoliths from deep fore-reef to shelf areas around Okinawa-jima, Ryukyu Islands, Japan. *Mar. Geol.*, **282**(3-4), 215–230.

McCaffrey, J.C., Wallace, M.W. and **Gallagher, S.J.** (2020) A Cenozoic Great Barrier Reef on Australia's North West shelf. *Global Planet. Change*, **184**. https://doi.org/10.1016/j.gloplacha.2019.103048

McKenzie, J.A., Hsü, K.J., Schneider, J.F., Zenger, D.H., Dunham, J.B. and **Ethington, R.L.** (1980) *Movement of Subsurface Waters Under the Sabkha, Abu Dhabi, UAE and its Relation to Evaporative Dolomite Genesis, Concepts and Models of Dolomitization*. SEPM Soc. Sed. Geol., pp. 20.

Medina-Elizalde, M. (2013) A global compilation of coral sea-level benchmarks: Implications and new challenges. *Earth Planet. Sci. Lett.*, **362**(0), 310–318.

Montaggioni, L.F. (2005) History of Indo-Pacific coral reef systems since the last glaciation: Development patterns and controlling factors. *Earth-Sci. Rev.*, **71**(1–2), 1.

Moore, C., Cappo, M., Radford, B. and **Heyward, A.** (2017) Submerged oceanic shoals of north Western Australia are a major reservoir of marine biodiversity. *Coral Reefs*, **36**(3), 719–734.

Mory, A.J. (1991) Geology of the Offshore Bonaparte Basin, Northwestern Australia. *Geol. Surv. W. Austr. Report*, **29**, 47 pp.

Murphy, R.J., Van Kranendonk, M.J., Baumgartner, R. and **Ryan, C.** (2021) Biogenicity of Spicular Geyserite from Te Kopia, New Zealand: Integrated Petrography, High-Resolution Hyperspectral and Elemental Analysis. *Astrobiology*, 115–135.

Murphy, R.J., Webster, J.M., Nothdurft, L., Dechnik, B., McGregor, H.V., Patterson, M.A., Sanborn, K.L., Webb, G.E., Kearney, L.I., Rintoul, L. and **Erler, D.V.** (2017) High-resolution hyperspectral imaging of diagenesis and clays in fossil coral reef material: a nondestructive tool for improving environmental and climate reconstructions. Geochem. Geophys. Geosyst., 18(8), 3209–3230.

Nicholas, W.A., Nichol, S.L., Howard, F.J.F., Picard, K., Dulfer, H., Radke, L.C., Carroll, A.G., Tran, M. and **Siwabessy, P.J.W.** (2014) Pockmark development in the Petrel Sub-basin, Timor Sea, Northern Australia: Seabed habitat mapping in support of CO2 storage assessments. *Cont. Shelf Res.*, **83**, 129–142.

Nothdurft, L.D. and **Webb, G.E.** (2009) Earliest diagenesis in scleractinian coral skeletons: implications for palaeoclimate-sensitive geochemical archives. *Facies*, **55**(2), 161–201.

O'Brien, G.W., Etheridge, M.A., Willcox, J.B., Morse, M., Symonds, P., Norman, C. and **Needham, D.J.** (1993) The structural architecture of the Timor Sea, North-Western Australia: implications for basin development hydrocarbon exploration. *The APPEA Journal*, **33**(1), 258–279.

O'Brien, G.W., Lisk, M., Duddy, I., Eadington, P.J., Cadman, S. and **Fellows, M.** (1996) Late Tertiary fluid migration in the Timor Sea: A key control on thermal and diagenetic histories? *The APPEA Journal*, **36**(1), 399–427.

O'Leary, M.J., Paumard, V. and **Ward, I.** (2020) Exploring Sea Country through high-resolution 3D seismic imaging of Australia's NW shelf: Resolving early coastal landscapes and preservation of underwater cultural heritage. *Quatern. Sci. Rev.*, **239**, 10.

OBIS (2020) OBIS (Ocean Bioversity Information System). https://obis.org/

Parker, J.H. (2009) Taxonomy of foraminifera from Ningaloo reef, Western Australia. *Assoc. Australs. Palaeontol. Mem.*, **36**. 767–784.

Patillo, J. and **Nicholls, P.J.** (1990) A tectonostratigraphic framework for the Vulcan Graben, Timor Sea region. *APPEA J.*, **30**(1), 27–51.

Paumard, V., Bourget, J., Durot, B., Lacaze, S., Payenberg, T., George, A.D. and **Lang, S.** (2019b) Full-volume 3D seismic interpretation methods: A new step towards high-resolution seismic stratigraphy. *Interpretation*, **7**(3), B33–B47.

Paumard, V., Bourget, J., Lang, S., Wilson, T., Riera, R., Gartrell, A., Vakarelov, B.K., O'Leary, M. and **George, A.** (2019a) Imaging past depositional environments of the North West Shelf of Australia: Lessons from 3D seismic data. In: *The Sedimentary Basins of Western Australia V: Proceedings of the Petroleum Exploration Society of Australia Symposium* (Ed. S.M.M. Keep), Petroleum Exploration Society of Australia., Perth, pp. 30.

Paumard, V., Bourget, J., Payenberg, T., Ainsworth, R.B., George, A.D., Lang, S., Posamentier, H.W. and **Peyrot, D.** (2018) Controls on shelf-margin architecture and sediment partitioning during a syn-rift to post-rift transition: Insights from the Barrow Group (Northern Carnarvon Basin, North West Shelf, Australia). *Earth-Sci. Rev.*, **177**, 643–677.

Payri, C., N'Yeurt, A. and **Orempuller, J.** (2000) *Algues de Polynésie française: Algae of French Polynesia*. Au Vent de Iles, Editions Tahiti, S.N. Des Editions Vilo, 320 pp.

Peltier, W.R. and **Fairbanks, R.G.** (2006) Global glacial ice volume and Last Glacial Maximum duration from an extended Barbados sea level record. *Quatern. Sci. Rev.*, **25**(23–24), 3322–3337.

Pico, T., Birch, L., Weisenberg, J. and **Mitrovica, J.X.** (2018) Refining the Laurentide Ice Sheet at Marine Isotope Stage 3: A data-based approach combining glacial isostatic simulations with a dynamic ice model. *Quatern. Sci. Rev.*, **195**, 171–179.

Precht, W.F. and **Aronson, R.B.** (2016) Stability of Reef-Coral Assemblages in the Quaternary. In: *Coral Reefs at the Crossroads* (Eds D.K. Hubbard, C.S. Rogers, J.H. Lipps, G.D. Stanley Jr.),. Springer, Netherlands: Dordrecht, pp. 155–173.

Purcell, P.G. and **Purcell, R.R.** (1988) The North West Shelf, Australia - An Introduction. In: *The North West shelf, Australia. Symposium*, 1988-08–10 (Eds P.G. Purcell and R.R. Purcell), PESA, Perth, pp. 3–15.

Renema, W. (2003) Larger foraminifera on reefs around Bali (Indonesia). *Zoologische Verhandelingen*, **345**(31), 337–366.

Renema, W. (2010) Is increased calcarinid (foraminifera) abundance indicating a larger role for macro-algae in Indonesian Plio-Pleistocene coral reefs? *Coral Reefs*, **29**(1), 165–173.

Renema, W. (2018) Terrestrial influence as a key driver of spatial variability in large benthic foraminiferal assemblage composition in the Central Indo-Pacific. *Earth-Sci. Rev.*, **177**, 514–544.

Renema, W. and **Troelstra, S.R.** (2001) Larger foraminifera distribution on a mesotrophic carbonate shelf in SW Sulawesi (Indonesia). *Palaeogeogr. Palaeoclimatol. Palaeoecol.*, **175**, 125–146.

Richards, Z. (2016) *The Coral Compactus: Western Australia; Hard Coral Genus Identification Guide*; Version 1.1. Publication URL: http://museum.wa.gov.au/explore/articles/wa-coral-compactus

Richards, Z., Beger, M., Hobbs, J.-P., Bowling, T., Chong-Seng, K. and **Pratchett, M.** (2009) Ashmore reef national nature reserve and Cartier island marine reserve marine survey 2009, Department of the Environment, Water Heritage & the Arts, JCU.

Rosenthal, Y., Holbourn, A.E., Kulhanek, D.K. and **Expedition 363 Scientists** (2018) Western Pacific Warm Pool. *Proceedings of the International Ocean Discovery Program*, **363**. http://publications.iodp.org/proceedings/363/363title.html

Salas-Saavedra, M., Dechnik, B., Webb, G.E., Webster, J.M., Zhao, J.-x., Nothdurft, L.D., Clark, T.R., Graham, T. and **Duce, S.** (2018) Holocene reef growth over irregular Pleistocene karst confirms major influence of hydrodynamic factors on Holocene reef development. *Quatern. Sci. Rev.*, **180**, 157–176.

Sanborn, K.L., Webster, J.M., Webb, G.E., Braga, J.C., Humblet, M., Nothdurft, L., Patterson, M.A., Dechnik, B., Warner, S., Graham, T., Murphy, R.J., Yokoyama, Y., Obrochta, S.P., Zhao, J.-X. and **Salas-Saavedra, M.** (2020) A new model of Holocene reef initiation and growth in response to sea-level rise on the Southern Great Barrier Reef. *Sed. Geol.*, **397**.

https://doi.org/10.1016/j.sedgeo.2019.105556.

Sandiford, M. (2007) The tilting continent: A new constraint on the dynamic topographic field from Australia. *Earth Planet. Sci. Lett*., **261**(1), 152–163.

Saqab, M.M. and **Bourget, J.** (2015) Controls on the distribution and growth of isolated carbonate build-ups in the Timor Sea (NW Australia) during the Quaternary. *Mar. Petrol. Geol*., **62**, 123–143.

Saqab, M.M. and **Bourget, J.** (2016) Seismic geomorphology and evolution of early–mid Miocene isolated carbonate build-ups in the Timor Sea, North West Shelf of Australia. *Mar. Geol*., **379**, 224–245.

Saqab, M.M., Bourget, J., Trotter, J. and **Keep, M.** (2017) New constraints on the timing of flexural deformation along the northern Australian margin: Implications for arc-continent collision and the development of the Timor Trough. *Tectonophysics*, **696–697**, 14–36.

Sarnthein, M., Grootes, P.M., Holbourn, A., Kuhnt, W. and **Kühn, H.** (2011) Tropical warming in the Timor Sea led deglacial Antarctic warming and atmospheric CO2 rise by more than 500yr. *Earth Planet. Sci. Lett*., **302**(3-4), 337–348.

Sasaki, K., Omura, A., Miwa, T., Tsuji, Y., Matsuda, H., Nakamori, T., Iryu, Y., Yamada, T., Sato, Y. and **Nakagawa, H.** (2006) 230Th/234U and 14C dating of a lowstand coral reef beneath the insular shelf off Irabu Island, Ryukyus, southwestern Japan. *Island Arc*, **15**(4), 455–467.

Sasaki, K., Omura, A., Murakami, K., Sagawa, N. and **Nakamori, T.** (2004) Interstadial coral reef terraces and relative sea-level changes during marine oxygen isotope stages 3–4, Kikai Island, central Ryukyus, Japan. *Quatern. Int*., **120**(1), 51–64.

Shuster, M.W., Eaton, S., Wakefield, L.L. and **Kloosterman, H.J.** (1998) Neogene Tectonics greater Timor Sea, offshore Australia: applications for trap risk. *The APPEA Journal*, **38**(1), 351–379.

Siddall, M., Rohling, E.J., Thompson, P.R. and **Waelbroeck, C.** (2008) Marine isotope stage 3 sea level fluctuations: Data synthesis and new outlook. *Rev. Geophys*., 46(RG4003,), doi:10.1029/2007RG000226.

Solihuddin, T., Bufarale, G., Blakeway, D. and **O'Leary, M.J.** (2016) Geomorphology and late Holocene accretion history of Adele Reef: a northwest Australian mid-shelf platform reef. *Geo-Mar. Lett*., **36**(6), 465–477.

Solihuddin, T., Collins, L.B., Blakeway, D. and **O'Leary, M.J.** (2015) Holocene coral reef growth and sea level in a macrotidal, high turbidity setting: Cockatoo Island, Kimberley Bioregion, northwest Australia. *Mar. Geol*., **359**, 50–60.

Strasser, A. and **Strohmenger, C.** (1997) Early diagenesis in Pleistocene coral reefs, southern Sinai, Egypt: response to tectonics, sea-level and climate. *Sedimentology*, **44**, 537–558.

Stuiver, M., Reimer, P.J. and **Reimer, R.W.** (2020) CALIB 8.2 [WWW program] at http://calib.org, accessed 2020-11-12.

Sturman, A. and **Tapper, N.** (2005) *The weather and climate of Australia and New Zealand*. Oxford University Press, Melbourne, 541 pp.

Stuut, J.-B.W., Temmesfeld, F. and **De Deckker, P.** (2014) A 550 ka record of aeolian activity near North West Cape, Australia: inferences from grain-size distributions and bulk chemistry of SE Indian Ocean deep-sea sediments. *Quatern. Sci. Rev*., **83**, 83–94.

Tager, D., Webster, J.M., Potts, D.C., Renema, W., Braga, J.C. and **Pandolfi, J.M.** (2010) Community dynamics of Pleistocene coral reefs during alternative climatic regimes. *Ecology*, **91**(1), 191–200.

Taylor, F.W., Mann, P., Bevis, M.G., Edwards, R.L., Cheng, H., Cutler, K.B., Gray, S.C., Burr, G.S., Beck, J.W., Phillips, D.A., Cabioch, G. and **Récy, J.** (2005) Rapid forearc uplift and subsidence caused by impinging bathymetric features: Examples from the New Hebrides and Solomon arcs. *Tectonics*, **24**(6), TC6005.

Thomas, A.L., Henderson, G.M., Deschamps, P., Yokoyama, Y., Mason, A.J., Bard, E., Hamelin, B., Durand, N. and **Camoin, G.** (2009) Penultimate Deglacial Sea-Level Timing from Uranium/Thorium Dating of Tahitian Corals. *Science*, **324**(5931), 1186–1189.

Toth, L.T., Aronson, R.B., Cobb, K.M., Cheng, H., Edwards, R.L., Grothe, P.R. and **Sayani, H.R.** (2015) Climatic and biotic thresholds of coral-reef shutdown. *Nature Climate Change*, **5**(4), 369–374.

Turner, J.A., Babcock, R.C., Hovey, R. and **Kendrick, G.A.** (2018) Can single classifiers be as useful as model ensembles to produce benthic seabed substratum maps? *Estuar. Coast. Shelf Sci*., **204**, 149–163.

Twiggs, E.J. and **Collins, L.B.** (2010) Development and demise of a fringing coral reef during Holocene environmental change, eastern Ningaloo Reef, Western Australia. *Mar. Geol*., **275**(1–4), 20–36.

van der Kaars, S. and **Deckker, P.** (2002) A Late Quaternary pollen record from deep-sea core Fr10/95, GC17 offshore Cape Range Peninsula, northwestern Western Australia. *Rev. Palaeobot. Palynol*., **120**, 17–39.

van der Kaars, S., De Deckker, P. and **Gingele, F.X.** (2006) A 100 000-year record of annual and seasonal rainfall and temperature for northwestern Australia based on a pollen record obtained offshore. *J. Quatern. Sci*., **21**(8), 879–889.

Verheij, E. (1994) Nongeniculate Corallinaceae (Corallinales, Rhodophyta) from the spermonde Archipelago, SW Sulawesi, Indonesia. *Blumea: Biodiver. Evol. Biogeogr. Plants*, **39**(1/2), 95–137.

Veron, J.E.N. and **Pichon, M.** (1979) Scleractinia of Eastern Australia. Part III Families Agariciidae, Siderastreidae, Fungiidae, Oculinidae, Merlinidae, Mussidae, Pectiniidae, Caryophylliidae, Dendrophylliidae. *Aust. Inst. Mar. Sci. Monogr*., **4**, 422 pp. DOI: https://doi.org/10.5962/bhl.title.60646

Veron, J.E.N. and **Stafford-Smith. M** (2000) *Corals of the world*. Aust. Inst. Mar. Sci. and CRR, 3 vols.

Veron, J.E.N. and **Wallace, C.** (1984) Scleractinia of Eastern Australia. Part V Families Acroporidae. *Aust. Inst. Mar. Sci. Monogr*., **6**, 485 pp.

Wallace, C. (1999) *Staghorn Corals of the World: A Revision of the Genus Acropora*. CSIRO Publishing, 421 pp..

Webster, J.M., Braga, J.C., Clague, D.A., Gallup, C., Hein, J.R., Potts, D.C., Renema, W., Riding, R., Riker-Coleman, K., Silver, E. and **Wallace, L.M.** (2009) Coral reef evolution on rapidly subsiding margins. *Global Planet. Change*, **66**(1–2), 129–148.

Webster, J.M., Braga, J.C., Humblet, M., Potts, D.C., Iryu, Y., Yokoyama, Y., Fujita, K., Bourillot, R., Esat, T.M., Fallon, S., Thompson, W.G., Thomas, A.L., Kan, H., McGregor, H.V., Hinestrosa, G., Obrochta, S.P. and **Lougheed, B.C.** (2018) Response of the Great Barrier Reef to sea-level and

environmental changes over the past 30,000 years. *Nature Geosci*., **11**(6), 426–432.

Weinmann, A.E., Rödder, D., Lötters, S. and **Langer, M.R.** (2013) Heading for New Shores: Projecting Marine Distribution Ranges of Selected Larger Foraminifera. *PLOS ONE*, **8**(4), e62182.

Whittam, D.B., Norvick, M.S. and **Mclntyre, C.L.** (1996) Mesozoic and Cainozoic Tectonostratigraphy of Western ZOCA and Adjacent Areas. *The APPEA Journal*, **36**(1), 209–232.

Woodroffe, C.D. and **Webster, J.M.** (2014) Coral reefs and sea-level change. *Mar. Geol*., **352**, 248–267.

Yokoyama, Y., Esat, T.M. and **Lambeck, K.** (2001) Coupled climate and sea-level changes deduced from Huon Peninsula coral terraces of the last ice age. *Earth Planet. Sci. Lett*., **193**(3-4), 579–587.

Yokoyama, Y., Esat, T.M., Lambeck, K. and **Fifield, L.K.** (2000) Last Ice Age Millennial Scale Climate Changes Recorded in Huon Peninsula Corals. *Radiocarbon*, **42**(3), 383–401.

Yokoyama, Y., Esat, T.M., Thompson, W.G., Thomas, A.L., Webster, J.M., Miyairi, Y., Sawada, C., Aze, T., Matsuzaki, H., Okuno, J.i., Fallon, S., Braga, J.-C., Humblet, M., Iryu, Y., Potts, D.C., Fujita, K., Suzuki, A. and **Kan, H.** (2018) Rapid glaciation and a two-step sea level plunge into the Last Glacial Maximum. *Nature*, **559**, 603–607.

Yokoyama, Y., Koizumi, M., Matsuzaki, H., Miyairi, Y. and **Ohkouchi, N.** (2010) Developing Ultra Small-Scale Radiocarbon Sample Measurement at the University of Tokyo. *Radiocarbon*, **52**(2), 310–318.

Yokoyama, Y., Miyairi, Y., Matsuzaki, H. and **Tsunomori, F.** (2007) Relation between acid dissolution time in the vacuum test tube and time required for graphitization for AMS target preparation. *Nuclear Instruments & Methods in Physics Research Section B-beam Interactions With Materials and Atoms*, **259**, 330–334.

Zhao, J.-x., Neil, D.T., Feng, Y.-x., Yu, K.-f. and **Pandolfi, J.M.** (2009) High-precision U-series dating of very young cyclone-transported coral reef blocks from Heron and Wistari reefs, southern Great Barrier Reef, Australia. *Quatern. Int*., **195**(1-2), 122–127.

Zuraida, R., Holbourn, A., Nürnberg, D., Kuhnt, W., Dürkop, A. and **Erichsen, A.** (2009) Evidence for Indonesian Throughflow slowdown during Heinrich events 3–5. *Paleoceanography*, **24**(2), PA2205.